UNIVERSITY OF CALIFORNIA, DAVIS

BERKELEY • DAVIS • IRVINE • LOS ANGELES • MERCED • RIVERSIDE • SAN DIEGO • SAN FRANCISCO SANTA BARBARA • SANTA CRUZ

DEPARTMENT OF MECHANICAL AND
AERONAUTICAL ENGINEERING
TELEPHONE: (530) 752-0580
FAX: (530) 752-4158
http://mae.engr.ucdavis.edu

ONE SHIELDS AVENUE
DAVIS, CALIFORNIA 95616-5294

DELINQUENT FINAL REPORT
Summary of Research

September 28, 2002

ATTN: Carol Dancy, Document Processing Section
NASA Center for AeroSpace Information (CASI)
7121 Standard Drive
Hanover MD 21076-1320

Dear Ms Dancy

This concerns NASA Cooperative Agreement NCC-1-01010. Enclosed are copies of two graduate theses completed under the identified agreement. Also enclosed are copies of three manuscripts that have also been completed under the agreement. These latter manuscripts are under review by, or will be submitted to, technical journals for publications. All these documents are intended to serve as the Summary of Research for the agreement identified above.

Sincerely,

Ronald A. Hess
Professor and Vice Chairman

cc: René H. Domino

Designing for damage – robust flight control design using sliding mode techniques

T. K. Vetter*, Wells, S. R.[§], and R. A. Hess*
*Department of Mechanical and Aeronautical Engineering, University of California, Davis, California, USA
[§]Department of Aeronautics, U.S. Air Force Academy, Colorado Springs, Colorado, USA

Abstract: A brief review of sliding model control is undertaken, with particular emphasis upon the effects of neglected parasitic dynamics. Sliding model control design is interpreted in the frequency domain. The inclusion of asymptotic observers and control "hedging" is shown to reduce the effects of neglected parasitic dynamics. An investigation into the application of observer-based sliding mode control to the robust longitudinal control of a highly unstable is described. The sliding mode controller is shown to exhibit stability and performance robustness superior to that of a classical loop-shaped design when significant changes in vehicle and actuator dynamics are employed to model airframe damage.

Keywords: sliding mode control, robust flight control, reconfigurable control,

1 INTRODUCTION

The performance demands of modern fighter aircraft has led to the introduction of vehicles with unstable bare-airframe dynamics exhibiting divergent modes beyond the control capabilities of the human pilot. The need for stability and command augmentation system (SCASs) in such vehicles is obvious. In addition, an emerging need for SCAS capabilities includes stability and performance robustness in the presence of airframe damage. In the military sector, a significant percentage of aircraft losses can be attributed to flight control damage such as loss of hydraulics, and actuator and control effector damage [1]. In the civilian sector, significant increases in air travel have been accompanied by a renewed interest in safety, including tolerance of an aircraft to damage and subsystem failure. The interest in flight safety and damage survivability has motivated research in failure/damage

tolerant flight control systems such as reconfigurable or restructurable flight control systems e.g., [2-5].

Most, if not all, reconfigurable or restructurable flight control system design techniques require one or more of the following: (1) failure detection/isolation, (2) control re-allocation, (3) parameter identification and (4) system reconfiguration. In applications involving aircraft with highly unstable modes, the time requirement for these may be prohibitive. Thus a scheme for designing SCASs that exhibit robustness to system failure/damage and that obviate operations (1) – (4) would be of definite interest. One such approach is that offered by Sliding Mode Control (SMC).

In its purest incarnation, SMC offers a control system with instantaneous and complete "adaptation" to what is termed matched uncertainty, i.e., SMC requires no failure detection/isolation, control re-allocation, parameter identification and system reconfiguration. The fundamental concepts describing SMC were first seen in the Russian literature in the 1930s. It was not until the 1970s that the ideas of SMC appeared in the Western literature when a text by Itkis [6], and a survey paper by Utkin [7] appeared. By the early 1990s, applications of SMC became numerous. These included robot control, motor control, and aircraft and spacecraft control. A recent text is devoted entirely to SMC design [8]. The next section will offer a brief overview of SMC concepts.

2 SLIDING MODE CONTROL

Consider the uncertain system with *m* inputs and *n* states given by:

$$\dot{\mathbf{x}}(t) = \mathbf{A}(\mathbf{x},t) + \mathbf{B}(\mathbf{x},t)\mathbf{u}(t) + \mathbf{D}\xi(\mathbf{x},t) \qquad (0)$$

where $\mathbf{A} \in \Re^{n\times n}$ and $\mathbf{B} \in \Re^{n\times m}$; **B** is full rank, $1 \le m < n$, and $R(\mathbf{D}) \subset R(\mathbf{B})$. The function $\xi : \Re_+ \times \Re^n \mapsto \Re^l$ is unknown an represents the parameter uncertainty or nonlinearities present in the system and is assumed to be bounded by some known functions of the state. The matrix $\mathbf{D} \in \Re^{n\times l}$ is known.

The obective is to define:

(a) m switching functions, represented in vector form as $\sigma(x)$ with the desired state trajectories

(b) a variable structure control

$$\mathbf{u}(\mathbf{x}, t) = \boldsymbol{\rho}\,\mathrm{sgn}(\boldsymbol{\sigma}) \tag{2}$$

such that any state outside the switching surface is driven to the surface in finite time and remains on this surface for all subsequent time (the so-called sliding mode). The line (or hypersurface) that describes $\sigma = 0$ defines the transient response of the system during the sliding mode (the so-called sliding surface). There are four basic properties about SMC that can be observed [**9**]:

(a) During the sliding mode, the trajectory dynamics are of a lower order than the original model.

(b) While on the sliding mode, the system dynamics are solely governed by the parameters that describe the line $\sigma = 0$ and are insensitive to the uncertain function $\xi(\mathbf{x},t)$ in Eq. 1

(c) The trajectory of the sliding mode is one that is not inherent in either of the two control structures alone.

It is item (b) immediately above that summarizes the invariance possible with SMC. Nothing has been said thus far about guaranteeing that the system will reach the sliding surface and remain on the surface once it is on it. Existence of the sliding mode requires stability of the state trajectory to the surface, or at least in some neighborhood surrounding the surface, known as the *region of attraction*. In order for the sliding surface to be attractive, the trajectories of $\sigma(t)$ must be directed towards it. This can be stated succinctly as requiring

$$\dot{\boldsymbol{\sigma}}^{\mathrm{T}}(t)\boldsymbol{\sigma}(t) < 0 \tag{3}$$

which is called the *reachability condition*

3 SLIDING MODE DESIGN

3.1 Multi-input, multi-output systems

There are many SMC design approaches in the literature. Indeed, an infinite variety of control strategies can achieve sliding behavior. The approach to be followed herein is based upon feedback linearization, as discussed in references **[10]** and **[11]**. Two major assumptions are involved in this approach:

(a) the system is square, - an equal number of inputs and outputs, and

(b) the system is feedback linearizable, - no transmission zeros in the right half plane and uncontrollable states must be stable.

If the system in question meets these criteria, it is possible to decouple the outputs with the given inputs. This transforms a multi-input, multi-output (MIMO) design into *m* simple single-input, single-output (SISO) designs, where *m* is the number of inputs or outputs. Consider a non-linear, square MIMO system

$$\begin{aligned} \dot{\mathbf{x}} &= \mathbf{f}(\mathbf{x}) + \mathbf{G}(\mathbf{x})\,\mathbf{u} \\ \mathbf{y} &= \mathbf{h}(\mathbf{x}) \end{aligned} \tag{4}$$

where $\mathbf{x} \in \Re^n$, $\mathbf{y} \in \Re^m$, $\mathbf{u} \in \Re^m$. Assume the functions $\mathbf{f}(\mathbf{x})$, $\mathbf{h}(\mathbf{x})$ and columns $g_i(\mathbf{x})$ $\forall i = \overline{1, m}$ of the matrix $\mathbf{G}(\mathbf{x}) \in \Re^{n\times m}$ are smooth vector fields. Further, assume the system is completely linearizable in a reasonable domain $x \in \Gamma$. The control system will be designed to track a real-time reference profile, $\mathbf{y}_r(t)$. This system can be transformed to a normal form **[11]**:

$$\begin{bmatrix} y_1^{(r_1)} \\ y_2^{(r_2)} \\ \cdots \\ y_m^{(r_m)} \end{bmatrix} = \begin{bmatrix} L_f^{r_1} h_1(x) \\ L_f^{r_2} h_2(x) \\ \cdots \\ L_f^{r_m} h_m(x) \end{bmatrix} + \mathbf{E}(\mathbf{x})\,\mathbf{u},$$

$$\mathbf{E}(\mathbf{x}) = \begin{bmatrix} L_{g_1}(L_f^{r_1-1}h_1) & L_{g_2}(L_f^{r_1-1}h_1) & \cdots & L_{g_m}(L_f^{r_1-1}h_1) \\ L_{g_1}(L_f^{r_2-1}h_2) & L_{g_2}(L_f^{r_2-1}h_2) & \cdots & L_{g_m}(L_f^{r_2-1}h_2) \\ \vdots & \vdots & \vdots & \vdots \\ L_{g_1}(L_f^{r_m-1}h_m) & L_{g_2}(L_f^{r_m-1}h_m) & \cdots & L_{g_m}(L_f^{r_m-1}h_m) \end{bmatrix} \qquad |\mathbf{E}(\mathbf{x})| \neq 0 \quad \forall x \in \Gamma \tag{5}$$

Where $L_f^{r_i}h_i$ and $L_{g_i}(L_f^{r_i-1}h_i)$ $\forall i = \overline{1,m}$ are corresponding Lie derivatives **[12]**. The superscripts appearing in Eq. (5) denote the "relative order" of the y_i and represent the order of the derivative of y_i necessary to ensure that a term containing an element of **u** appears.

Next design *m* independent sliding surfaces (note, these have orders exactly one less than the relative order for the corresponding state variable):

$$\sigma_i = e_i^{(r_i-1)} + c_{i,r_i-2}e_i^{(r_i-2)} + \ldots + c_{i,1}e_i^{(1)} + c_{i,0}e_i \quad \forall i = 1,m \tag{6}$$

where $e_i = y_{r,i}(t) - y_i(t)$, $e_i^{(j)} = \frac{d^j e_i}{dt^j}$. The coefficients $c_{i,j}$, $\forall i = 1,m$ and $\forall j = 0, r_i - 2$, are design parameters which can be chosen in a number of ways, e.g., to achieve the desired eigenvalue placement of the decoupled differential equations of the output variables. In a later section, a frequency-domain approach to the selection of the c_i will be presented. It is also common to include an integral term, $c\int e_i d\tau$, in the sliding equations to account for potential steady state error which can occur when utilizing a sliding mode boundary layer. The control law that can be used is

$$u_i = \rho_i \, \mathrm{sgn}(\sigma_i) \tag{7}$$

In order to prove system stability, assume the candidate Lyapunov function $V_i = 0.5\sigma_i^2$, take the derivative of the sliding functions, σ_i, and solve for ρ_i which provides global attractiveness to the sliding surface in finite time.

3.2 Implementation Issues

While very attractive from a robustness standpoint, serious implementation issues must be addressed in SMC applications. The most serious of these issues is the infinite frequency switching that occurs when the control law of Eq. 7 is used in a control system. The switching has been called "chatter" by some researchers, although, strictly speaking, chatter refers to a related (and undesirable) phenomenon in which the state trajectories chatter along the sliding manifold. The simplest and most common approach to the elimination of infinite frequency switching in the control law is use of the so-called boundary layer in which the signum function of Eq. 7 is replaced by an approximation, e.g., a saturation element. The result of using such an element is that the control becomes continuous and the states become attracted to a small boundary layer surrounding the switching surface. Since the ideal sliding motion is lost, the resulting system is often referred to as pseudo-sliding. In addition, when a boundary layer is introduced, invariance is lost, although the system still

retains much of its robustness. It is this latter issue, ensuring that sufficient robustness remains in the design, that constitutes the major challenge of the research to be described.

3.3 Unmodeled parasitic dynamics

Unmodeled parasitic dynamics refers to dynamics of the vehicle that are typically neglected in the design procedure. These can include actuator dynamics and aeroelastic modes. Unfortunately, SMC designs are very sensitive to the effects of unmodeled parasitic dynamics [**13**].The simplest solution to the actuator problem would appear to be the inclusion of the actuator in the model of the vehicle dynamics. However, including actuator dynamics will increase the relative orders of the system, and, as Eq. 6 indicates, the order of the manifolds. This means, for example, for a second order actuator, at least two derivatives of the system output will be required. In practice, measurement noise makes this approach very unattractive. As will be seen in a later section, using reduced order actuator models in the design is a viable alternative to either neglecting the actuator dynamics altogether, or incorporating the full models of these elements in the design.

A number of approaches have been offered in the literature for dealing with the effects of parasitic dynamics. These include

(a) dynamic boundary layers in which the boundary layer thickness is continuously adjusted to keep the controller operating in the linear region,

(b) disturbance compensation in which an SMC disturbance estimator is employed,

(c) SMC design with a prefilter in which actuator dynamics are incorporated as a prefilter to the SMC

(d) observer-based SMC in which an asymptotic observer is placed in the feedback path for the SMC.

The observer-based approach will be adopted in the research to be described. This decision was based upon the relative simplicity of this technique and the fact that it is easily amenable to a frequency domain description. As will be demonstrated, separate observers for each feedback variable (each decoupled control loop in a MIMO system) can be employed in the design. The selection of observer eigenvalues is governed by the following guidelines: Large observer eigenvalues (a "fast" observer) increases the robustness of the

SMC design to variations in vehicle characteristics but also increases the susceptibility of the design to the deleterious effects of unmodeled parasitic dynamics. Small observer eigenvalues (a "slow" observer) decreases the robustness of the SMC design to variations in vehicle characteristics, but also decreases the susceptibility of the design to the effects of unmodeled parasitic dynamics. To allow large observer eigenvalues while minimizing susceptibility to parasitic dynamics the SMC approach to be followed will utilize "model reference hedging" [**14**]. In its initial incarnation, this hedging involved passing the control signal **u** through a model of the vehicle that contained no parasitic dynamics and subtracting the resulting signal from the measured vehicle output. The resulting "error" signal represents the amount of unachieved performance due to the parasitic dynamics. This error signal is multiplied by a gain and subtracted from the output of the reference model $\mathbf{y}_r(t)$ that the SMC system is to follow. The term "hedging" derives from the fact that the reference model output is modified (hedged) by a signal reflecting the importance of unmodeled parasitic dynamics. As will be seen, this hedging concept will be generalized and, like the observer design, interpreted in the frequency domain.

3.4 The Equivalent Plant

Figure 1 shows a MIMO control system including the asymptotic observers and reference model hedging as just outlined. Figure 2 is a modification of Fig. 1 in which the reference model hedging is shown in equivalent form as an additional feedback loop in parallel with the observers. In Fig. 2, G_h represents a model of the vehicle. In the frequency domain approach to be described, G_h is generalized and simplified to the following form:

$$G_h = \frac{a_0}{(s^{r_i+1} + a_{r_i} s^{r_i} + \cdots + a_0)} \tag{8}$$

where r_i is the relative order of the output variable of interest. Likewise, the filter G_f is a high-pass filter of the form

$$G_f = \frac{s}{s+b} \tag{9}$$

Parameter selection in Eqs. 8 and 9 is based upon a Bode diagram of the hedge transfer function $\hat{y}_h / y_c$ [**14**]. Referring to Fig. 2, $G_f G_h$ is created so that the magnitude portion of its Bode diagram exhibits the following characteristics: a +20 dB/dec slope at low

frequencies, a $-20r_1$ dB/dec slope at frequencies where the (neglected) actuator dynamics distort the magnitude curve of $\hat{y}_h / y_c$, (r_1 = the relative order of system without parasitic dynamics) and a $-20(r_1-1)$ dB/sec slope at high frequencies. The gain K_h is then varied until the transfer function $\hat{y}_h / y_c$ in Fig. 2 closely approximates that for the vehicle without parasitic dynamics while employing as large as eigenvalues as possible in the corresponding observer.

The system of Fig. 2 can be simplified to that of Fig. 3 in which the original vehicle, actuator models, observers and hedging dynamics are replaced by an "equivalent" plant $\mathbf{P_e}$ [**14**]. The goal of the loop shaping procedure just described involving observers and hedging is simply to create an effective plant $\mathbf{P_e}$ whose Bode plot resembles that of the vehicle without parasitic dynamics. In doing this, much of the robustness of the original SMC design can be regained.

4. DESIGN EXAMPLE

4.1 Vehicle Model

The SMC design approach outlined in general terms in the previous sections is best presented in detail by means of an example. The aircraft model in question describes the longitudinal dynamics of a forward swept wing aeroelastic vehicle as developed in Ref. [**15**]. The model of Ref. [**15**] is extended here to include thrust effects. Figure 4 shows the general vehicle configuration. The linearized vehicle dynamics are given below for a flight condition of steady, wings-level flight at sea level at a trim airspeed of 1000 ft/s. The state variables in the model are defined as

$$\mathbf{x}(t) = [a(t), \alpha(t), \theta(t), q(t), \eta_1(t), \dot{\eta}_1(t), \eta_2(t), \dot{\eta}_2(t)]^T \qquad (10)$$

where

$a(t)$ represents airspeed deviation from trim, ft/s

$\alpha(t)$ represents angle attack deviation from trim, rad

$\theta(t)$ represents pitch attitude deviation from trim, rad

$q(t) = \dot{\theta}(t)$ represents pitch rate, rad/s

$\eta_1(t)$ = generalized coordinate for wing bending mode

$\eta_2(t)$ = generalized coordinate for wing torsion mode

The control variables are defined as

$$\mathbf{u}(t) = [\delta_c(t), \delta_t(t), \delta_f(t)]^T \tag{11}$$

where

$\delta_c(t)$ = canard deflection, rad (positive leading edge up)

$\delta_t(t)$ = thrust change, lbf

$\delta_f(t)$ = flaperon deflection, rad (positive trailing edge down)

The vehicle model for two different center of gravity (cg) locations is given below, with subscripts 'a', 'c' and denoting aft, and center cg locations, respectively.

$$A_a = \begin{bmatrix} 6.6355E-4 & 10.19 & -32.2 & -16.24 & -0.2674 & 2.890E-3 & 5.261 & 3.806E-5 \\ -6.438e-5 & -2.881 & -5.2316E-4 & 1.010 & 7.627E-2 & -8.182E-4 & -1.489 & -1.077E-5 \\ 0 & 0 & 0 & 1 & 0 & 0 & 0 & 0 \\ 2.534e-6 & 119.9 & 2.053E-5 & -1.086 & -2.122 & 2.907E-2 & 45.85 & 1.609E-3 \\ 0 & 0 & 0 & 0 & 0 & 1 & 0 & 0 \\ -1.122 & -31800 & -8.45E5 & 103.8 & -3624 & -20.64 & -28050 & 3.852E-2 \\ 0 & 0 & 0 & 0 & 0 & 0 & 0 & 1 \\ 1.039e-2 & 75.20 & -1.95E-5 & -0.7286 & -7.574E-2 & -8.238E-4 & -45240 & -3.6E-2 \end{bmatrix} \quad B_a = \begin{bmatrix} 1.804 & 0.002 & 6.654 \\ -0.5108 & 0 & -0.4627 \\ 0 & 0 & 0 \\ 68.48 & 0 & -12.97 \\ 0 & 0 & 0 \\ 281.6 & 0 & -6200 \\ 0 & 0 & 0 \\ 64.93 & 0 & 1.337 \end{bmatrix}$$

$$A_c = \begin{bmatrix} 5.266E-4 & 5.315 & -32.2 & -14.53 & -0.1405 & 1.507E-3 & 2.743 & 1.984E-5 \\ -6.438e-5 & -2.881 & -4.672E-4 & 1.006 & 7.627E-2 & -8.182E-4 & -1.489 & -1.077E-5 \\ 0 & 0 & 0 & 1 & 0 & 0 & 0 & 0 \\ 2.033e-6 & 79.56 & 1.457E-5 & -0.8311 & -1.055 & 1.762E-2 & 25.01 & 1.458E-3 \\ 0 & 0 & 0 & 0 & 0 & 1 & 0 & 0 \\ -0.9439 & -31160 & -6.779E-5 & 66.40 & -3624 & -20.64 & -28050 & 3.855E-2 \\ 0 & 0 & 0 & 0 & 0 & 0 & 0 & 1 \\ 3.363e-3 & 75.09 & -1.564E-5 & -0.645 & -7.6254E-2 & -8.13E-4 & -45240 & -3.6E-2 \end{bmatrix} \quad B_c = \begin{bmatrix} 0.9407 & 0.002 & 5.871 \\ -0.5108 & 0 & -0.4627 \\ 0 & 0 & 0 \\ 61.33 & 0 & -19.44 \\ 0 & 0 & 0 \\ 281.7 & 0 & -6200 \\ 0 & 0 & 0 \\ 64.99 & 0 & 1.338 \end{bmatrix}$$

(12)

The control surface actuator dynamics and simplified engine model are given below, along with associated position and rate limits.

	Dynamics	Position Limits	Rate Limits
Canard	$\frac{70^2}{s^2+2\cdot 0.7\cdot 70\cdot s+70^2}$	±15 deg	100 deg/s
Engine	$\frac{1}{s+1}$	n/a	n/a
Flaperons	$\frac{35^2}{s^2+2\cdot 0.7\cdot 35\cdot s+35^2}$	±35 deg	60 deg/s

As an example, the aeroelastic characteristics of the vehicle with the center cg location have the following modal properties:

wing bending mode: $\omega_n = 60$ rad/s $\quad \zeta = 0.165$

wing torsional mode: $\omega_n = 213$ rad/s $\quad \zeta = 8 \cdot 10^{-5}$

The SMC design, itself, will be based upon the center cg location model neglecting structural modes. The aft cg configuration, however, will be included in a computer simulation of the resulting vehicle and SCAS. It should be noted that this vehicle is highly unstable. For example, with the center cg location, the longitudinal dynamics exhibit an aperiodically divergent mode with a time to double amplitude of 0.094 s. With the aft location the time to double amplitude of the unstable mode decreases to 0.087 s.

Measurement noise will be included in a computer simulation of the system. The measurement noise models consist of filtered white noise, with the filter dynamics given by

$$N(s) = \frac{20^2}{(s^2 + 2(0.707)20s + 20^2)} \tag{13}$$

The white noise power was adjusted to yield root-mean-square (RMS) values of the measured variables of 0.25 deg/s for q(t) and 25 ft/s for a(t).

4.2 SMC Reference Model

The SCAS will be a pitch-rate command and airspeed-hold system, with the pilot controlling pitch attitude through pitch-rate. The reference model for the pitch-rate command system is

$$G_r(s) = \frac{q}{q_c}(s) = \frac{10^2}{(s^2 + 2(0.707)10s + 10^2)} \tag{14}$$

Using a pilot modeling approach discussed in Ref. **[16]**, these dynamics are predicted to yield Level 1 handling qualities with no pilot-induced oscillation (PIO) tendencies. Since the airspeed loop was not a command-response system, no airspeed reference model was needed.

4.3 SMC Design Procedure

The SMC design procedure can now be presented in step-by-step fashion. As part of the procedure below, one creates a computer simulation of the system. Here, this is accomplished using MATLAB® and Simulink®. The steps below are directed toward the single loop of a SISO system or any single loop of a MIMO system. In either case, only a scalar sliding surface definition is involved.

(1) Plant Definition: A vehicle model is chosen. It may or may not include a reduced- first order actuator model per the designer's choice. This decision will be treated in the following discussion. A 'limit frequency' is defined above which parasitic dynamics, and unstructured uncertainties become a concern.

(2) Reference Model: A reference model is chosen. Since this study is directed toward achieving piloted flight, a reference model which will produce a Cooper-Harper rating of Level 1 with no PIO tendencies should be selected.

(3) Sliding Surface Definition: The desired feedback structure is determined, e.g., a pitch rate command system. If there are multiple actuators per pseudo-control produced by the SMC system, a control distribution matrix must be created by any number of methods, e.g., the pseudo-inverse approach of Ref. [**14**]. The sliding manifold can then be created using the following rules:

(a) σ is derived from a tracking error expression Eq. 6 where here r_i is the relative order of the system for the output being considered. Note that the $(r_i\text{-}1)^{st}$ derivative of the error signal is used in the definition of σ. Also an integral term is also included compensating for the addition of the boundary layer.

$$\sigma = e(t)^{r_i-1} + c_{r_i-2}e(t)^{r_i-2} + \ldots + c_0 e(t) + c_{-1}\int e(t)dt \tag{15}$$

(ii) Equation 13 can be transformed to the Laplace domain and expressed as

$$u(s) = \frac{\rho}{\varepsilon}\sigma = K_\rho\left(s^{r_i-1} + c_{r_i-2}s^{r_i-2} + \ldots + c_0 + \frac{c_{-1}}{s}\right)e(s) \tag{16}$$

In the frequency domain, the c_i are chosen to produce broad K/s properties around crossover in the loop transmission. This will always be possible to achieve since enough derivatives are included in Eq. 15 (and powers of s in Eq. 16) to produce the desired shape at frequencies at least as high as the limit frequency. K_ρ is also obtained in this step to set the crossover frequency. Since the signum function will be replaced by a saturation element with a $\pm$ 1 limit, K_ρ represents the largest possible control output of the SMC. Thus, to use the entire range of the actuator suite in question, the minimum K_ρ must be equal to or greater than the position limit of the actuator in the suite with the largest position limit. Also note that the crossover frequency obtained in this will typically be very large and well beyond the limit frequency. This is of no concern at this juncture.

(4) Sliding Behavior: The existence of the sliding mode is now be confirmed. Here the signum function is used without a boundary layer in a Simulink® simulation of the system. A reaching phase followed by infinite switching should be observed in addition to $\sigma(t) = 0$ for $t > t_s$ where t_s is at the zero crossing of σ. Note that an observer, additional actuator orders, reference models, and hedging have not yet been added and there are no outer loop closures. If sliding behavior (infinite switching and $\sigma(t) = 0$ for $t > t_s$) is not observed, K_ρ is increased until it is.

(5) Boundary Layer: Now a boundary layer is introduced via the saturation element with unity limits. The boundary layer thickness ε is increased until no infinite switching is observed while maintaining near perfect tracking as seen in $\sigma(t) \approx 0$. This should be possible even with large variations in plant dynamics. Modifying ρ may be necessary in this step. If ε increases above 1 then increase ρ to maintain a constant $\rho/\varepsilon=K_\rho$.

(6) Parasitic Dynamics: The dynamics of the operational actuators are now included in the Simulink® simulation of the system. This will almost surely cause the system to be unstable.

(7) Observers: The design of the observers is of critical importance to the tracking performance and robustness of the entire system. The poles of this observer should be chosen to lie between the limit frequency and the bandwidth of the reference model. In

the MIMO case, an independent observer on each feedback channel can significantly improves tracking and robustness by allowing different observer eigenvalues in each loop.

(8) Hedging: The model reference hedging is designed in the frequency domain as described in Section 3.4

(9) Reduced-order Model Actuators: If desired, if not included in step (1), actuator models may be included in the design, but of lower order than the actual, operational actuators. Steps (3)-(8) are repeated. As a rule of thumb, the bandwidth of the lower-order actuators should be chosen to be approximately 60% of the operational ones. This step may improve system robustness by including a lower-order model of parasitic dynamics without requiring excessive differentiation of the error signal in the sliding surface definition of Eq. 15.

4.4 Pilot Model

A control theoretic model of the human pilot was included in the Simulink® simulations to be described. This model was compensatory in nature and assumed that the pilot was following some commanded pitch-attitude time history, e.g., that commanded on a head-up display unit in the cockpit. The pilot model was the Structural model as described in Ref. **[16]**, and included a model for a cockpit force-feel system given by

$$Y_{FS} = \frac{25^2}{s^2 + 2(0.707)25s + 25^2} \tag{17}$$

The Structural pilot modeling procedure includes a normalization process so that the eliminates any dependence upon units associated with Y_{FS}. The pilot model controls only vehicle pitch attitude, with the airspeed-hold feature of the control system design maintaining a desired trim airspeed. The resulting pilot model is shown in Fig. 5 and was obtained assuming that the dynamics between the pilot's control input and the resulting pitch rate were determined by the reference model given in Eq. 14. The crossover frequency for the inner pilot/vehicle control loop was selected as 1.5 rad/s.

4.5 Design Details – Nominal Vehicle (Center CG Location)

4.5.1 Control Distribution, Sliding Surface, Observer and Hedging Definitions

The control distribution matrix for the design was chosen as:

$$K = \begin{bmatrix} 1 & 0 \\ 0 & 1 \\ -1 & 0 \end{bmatrix} \tag{18}$$

This means that the SMC pseudo-command for pitch rate will be distributed uniformly to both the canard and flaperon. The negative sign arises because of the fact that pitching moments of opposite sign arise from positive deflections of the canard and flaperon. The distribution of Eq. 19 was chosen for simplicity.

Figure 6 shows the architecture for complete pilot/vehicle system. For the purposes of this design, lower (first)-order actuator dynamics will be assumed for the canard and flaperon. The actuator for the thrust, was, however, neglected in the design. as suggested in Step (j) of Section 4.3. Figure 7 shows the Bode plot of the q/u_{cq} transfer function for the vehicle with assumed first-order actuators for the canard and flaperon but no aeroelastic modes. Using the 60% bandwidth figure cited in design step 9 of Section 4.3, these actuators have the form:

$$\text{Canard: } \frac{42}{(s+42)} \qquad \text{Flaperon } \frac{21}{(s+21)} \tag{19}$$

The –40 dB/dec slope of the magnitude curve at high frequencies in Figure 7 indicates that the relative order $r_q = 2$. Thus, Eq. 16 becomes

$$u(s) = \frac{\rho}{\varepsilon}\sigma = K_\rho\left(s + c_0 + \frac{c_{-1}}{s}\right)e(s) \tag{20}$$

Note that Eq. 20 takes the form of a simple proportional, integral, derivative (PID) controller. As outlined design steps (3)-(8) in Section 4.3, selection of c_0 and c_{-1} is done through loop shaping to the produce broad K/s properties around crossover in the loop transmission. Figure 8 shows the resulting loop transmission with a crossover frequency

chosen as 100 rad/s. The caveat regarding high crossover frequencies that was mentioned in design step (3-b) is pertinent at this juncture. Equation 20 now takes the form

$$u(s) = \frac{\rho}{\varepsilon}\sigma = 0.02\left(s + 80 + \frac{700}{s}\right)e(s) \tag{21}$$

The existence of sliding behavior is now established through a Simulink® simulation of the system. Here, the reference model is ignored and the input to the SMC system is chosen as a sum of sinusoids

$$q_c = \sum_{i=1}^{7} A_i \sin(\omega_i t) \tag{22}$$

with an RMS value of approximately 4 deg/s. It was found that K_ρ had to be increased from the value in Eq. 21 to $K_\rho = 0.04$. Finally, to ensure that the limiting value of K_ρ corresponded to the largest of the position limits of the actuators serviced by u_{cq}, (35 deg for the flaperon actuator), K_ρ was increased to $K_\rho = 0.6$.

With the q-loop closed with the continuous control of Eq. 21, the airspeed-loop compensation was designed. No SMC system was incorporated for the airspeed loop, since this was a low-bandwidth system. The airspeed compensation was created as

$$G_{c_a} = \frac{\delta_{t_c}}{a} = 500 \text{ lbf}/(\text{ft}/\text{s}) \tag{23}$$

and resulted in a 1 rad/s crossover frequency in the airspeed loop.

A boundary layer for the q – loop was now created by replacing the signum element with a saturation element and replacing K_ρ by ρ/ε. It was found that $\varepsilon = 1.0$ eliminated the infinite frequency switching behavior and did not require any modification of ρ as discussed in design step (5) of Section 4.3. Following design step (6), parasitic dynamics are now added to the Simulink® simulation and instability results. This is to be expected.

Separate observers were next designed for the airspeed and pitch-rate loops. The eigenvalues for each observer were set to the limit frequencies for each control loop as defined in design step (1). These were defined as 30 rad/s for the q-loop and 1 rad/s for the airspeed loop. These values corresponded to the minimum undamped natural frequenices of

the actuators servicing u_{cq} and u_a, the two pseudo-controls. To avoid numerical problems with the observer design, the eigenvalues were seperated as follows:

$$q-\text{loop}: \quad \lambda = -30, -31, -32, -33; \quad a-\text{loop}: \ \lambda = -1 \qquad (24)$$

Note that in Fig. 6, the reduced-order actuator models are explicitly included in the observer loop. Hence the number of eigenvalues for the q – loop is four, the order of the vehicle dynamics, excluding actuators and aeroelastic modes. The single eigenvalue for the airspeed-loop observer is based upon a simplifed, low-frequency model of the airspeed to throttle dynamics of the vehicle with the high-frequency q – loop closed via the linear compensation of Eq. 21. Figure 9 shows the effect of various eigenvalue ranges on the transfer function $\hat{q}/u_{cq}$.

Model reference hedging was next designed for the q – loop. The effects of this hedging are shown in Fig. 10. The hedging function is denoted $K_hG_hG_f$ as described in Section 3.4 and shown in Fig. 3. Here,

$$K_hG_hG_f = \frac{(K_h)s}{(s+20)(s+45)^2(s+80)} \qquad (25)$$

By increasing K_h in Eq. 25, the magnitude of the $K_hG_hG_f$ Bode plot, translates vertically. In doing so, the magnitude and phase distortion of the $\hat{q}/u_{cq}$ Bode plot evident in Fig. 9 can be reduced considerably compared to that for the vehicle with no parasitic dynamic, as Fig. 10 indicates. Figure 11 shows the final $K_hG_hG_f$ and $\hat{q}/u_{cq}$ Bode plots. The results presented in Fig. 11 are of central importance to the design. The figure indicates that the combination of linear asymptotic observers and reference model hedging has created an equivalent plant (see Fig. 3) that closely approximates that of the actual vehicle without the parasitic dynamics associated with the actuators. This, in turn, allows the SMC system to retain much of its robustness, and does so without higher-order error signal differentiation that would be necessary if the full-order actuator models were included in the design.

4.5.2 Damage Definitions

4.5.2.1 Damage Condition 1

The "damage" to the aircraft in this example will be modeled by as follows: The canard and flaperon actuators will operate with 0.025 s time delays in their dynamics. In addition, the actuator effectiveness (gain) will be reduced by 50%. Excluding elements describing kinematic relationships, each element of the **A** and **B** state description of the vehicle will be perturbed by ± 20%. Using the **A** matrix as an example, this perturbation is implemented as follows:

$$\mathbf{A}_{\text{damage}}(i, j) = \mathbf{A}(i, j)[1 + 0.2(-1)^j] \tag{26}$$

Obviously, these changes do not accurately describe any particular damage scenario. They were selected for ease of implementation and the maintenance of linearity for the purposes of exposition in the frequency domain to be discussed in the following section.

4.5.2.2 Damage Condition 2

An additional damage scenario will be briefly considered that will not be included in the analyses to follow, but will be simulated. In this damage, no delays or gain reductions are considered in the actuators, but the flaperon will jam at $\delta_f = 5$ deg. The 20% changes in the non-kinematic elements of the vehicle **A** and **B** matrices are retained.

4.5.3 Stability Margins and Measurement Noise Amplification

Figures 12 and 13 show the loop transmissions that result from the complete system of Fig. 6 (without the pilot) when the loops are broken, in turn, at the input to the canard and flaperon actuators respectively. Results for the nominal (undamaged, center cg location) vehicle and that with damage condition 1 are shown. This stability analysis is not as rigorous as one obtained by inserting a perturbation matrix of the form

$$\mathbf{P} = \text{diag}(K_1 e^{-j\phi_1}, K_2 e^{-j\phi_2}) \tag{27}$$

before the actuators and assessing closed-loop stability when K_i and ϕ_i are varied within some desired region in the gain and phase parameter space. The single-loop approach was adopted for the sake of simplicity here. As the figures, indicate, adequate stability margins

are in evidence for the loop cut before the flaperon actuator, but the margins are small for the damaged vehicle, with the loop cut before the canard actuator. These small margins are attributable to the severity of the modeled damage and to the power of the canard effector.

Figure 14 shows the magnitudes of the transfer functions between the pseudo-controls u_{cq} and u_{ca} and noise signals injected in parallel with the measured vehicle outputs pitch-rate q(t) and airspeed a(t) for the nominal vehicle and that with damage condition 1. As the figure indicates, noise amplification due to q_{noise} is significant at high frequencies for both nominal and damaged vehicles. This amplification is attributable to the derivative term in the PID controller of Eq. 21, which in turn derives from the inclusion of first-order actuator models in the SMC design.

4.5.4 Equivalent Loop Transmissions

Is it useful to obtain an equivalent loop transmission for the q-loop of the SMC design for the purposes of comparison with a classical design to be presented in the next section. First, a closed-loop transfer function is obtained as

$$G = \left.\frac{q}{q_c}\right|_{a \to \delta_t} \tag{28}$$

where q_c is the output of the reference model of Fig. 6 and the notation $a \to \delta_t$ indicates that the airspeed loop is considered closed in the calculation of G. Now Eq. 28 can also be written

$$G = \frac{L_{equiv}}{1 + L_{equiv}} \tag{29}$$

where L_{equiv} is the loop transmission of an equivalent unity-feedback system that has the same closed-loop transfer function as that of the SMC system. This L_{equiv} is equivalent to the y/e transfer function from Fig. 3. Equation 29 can be rewritten as

$$L_{equiv} = \frac{G}{1 - G} \tag{30}$$

Figures 15 shows the L_{equiv} for the SMC nominal vehicle and that with damage condition 1. Note, again that while positive stability margins are in evidence for both vehicles, those

associated with the damaged vehicle have been significantly reduced. In addition, the lower crossover frequency of the damaged system will have repercussions in terms of predicted handling qualities, as will be seen in a later section. The reader will note the very high crossover frequency of the L_{equiv} for the SMC system of approximately 100 rad/s.

4.5.5 Classical Loop-Shaping Design

To provide a meaningful assessment of the performance and robustness benefits of the SMC design just presented, a comparison design was created. This design was obtained through classical loop shaping procedures using fixed compensators in the forward loops of the square feedback system controlling pitch rate and airspeed. The airspeed compensation for the classical design was identical to that for the SMC system. The q-loop compensation is given by

$$\frac{u_{eq}}{q_c - q} = \frac{0.5(s+0.1)(s+10)^2}{s^2(s+2.2)} \tag{31}$$

Figure 16 compares the L_{equiv} transfer functions obtained using Eq. 31 for the classical and SMC designs for the nominal vehicle. As can be seen from the figure, the L_{equiv} for the SMC system exhibits a larger crossover frequency and significantly less phase lag than the classical design.

4.6 Simulated Pilot/Vehicle Performance

The theta command for the pilot/vehicle system was chosen as a series of filtered pulses ± 5 deg in magnitude, with each pulse lasting 5 s. To demonstrate the system robustness, the undamaged vehicle model is chosen as that corresponding to the aft cg position, rather than the center position used in the design. The actual second order actuators are included, as well as the aeroelastic modes. Finally, an unmodeled 0.015 s time delay was included in the measurements of q(t) and a(t). The "damage" described in the previous section was introduced 20 s into a Simulink® simulation of the pilot/vehicle system. Note that no changes in the pilot model dynamics are considered after failure. While a human pilot can adapt to changes in vehicle characteristics, the conservative assumption made here is that stability and performance robustness of the SCAS should be in evidence in the absence of such changes. Simulation results for both the SMC and classical designs will be presented.

Figure 17 shows the pitch-attitude pilot/vehicle tracking performance for the SMC design in damage condition 1. As can be seen, there is little degradation in performance after the damage at 20 s. Figure 18 shows the corresponding airspeed deviations from trim, while Figs. 19 and 20 show the canard and thrust time histories, respectively. Because of the control allocation of Eq. 18, the flaperon time history is essentially the negative of that of the canard. Figure 21 shows the pitch-attitude pilot/vehicle tracking performance for the classical design. Note that almost immediately after the damage, the system goes unstable. Figure 22 shows the canard time history, with the instability readily apparent. The comparisons between the SMC and classical designs clearly demonstrate the superiority of the SMC design as regards stability and performance robustness.

Figure 23 shows the pitch-attitude pilot/vehicle tracking performance for the SMC design for damage condition 2. Again, little degradation in performance occurs after the damage at 20 s. Figures 24 and 25 show the canard and flaperon time histories, respectively. While not shown, the classical design immediately went unstable with this failure.

4.7 Handling Qualities Predictions

The fact that the vehicle damage considered in the previous sections could be described by linear systems allows the prediction of handling qualities. Here Bandwidth/Phase Delay was selected as the analysis metric [17]. The calculations were carried out including the dynamics of the force-feel system, as suggested in Ref. [17]. Figure 26 shows the boundaries of this metric and the Bandwidth/Phase Delay points for the configurations examined in the previous section. All points were calculated at the off-design, aft-cg position. No points were plotted for the classical design in either damage conditions, since the simulated pilot/vehicle system was unstable. As can be seen, the damage conditions significantly degrade handling qualities of the vehicle, even with the SMC design. This is particular true for damage condition 1. This latter result is, of course, attributable to the severity of the modeled damage, in particular the total 40 ms additional time delay that occurs in the control loop.

5 EXTENSION TO MIMO SYSTEMS

As Ref. [**14**] demonstrates, extension of the SMC design technique presented here to MIMO systems is straightforward. Assuming a square, feedback linearizable control system, each loop is treated as a SISO system. The only added complexity occurs through the possible necessity of cross-hedging, i.e., feeding hedged signals between different control loops. However, the technique of determining the form and the gain of the hedging is the same as for SISO systems.

6 CONCLUSIONS

Based upon the research that has been described, the following conclusions can be drawn:

(1) A practical flight control system design methodology is feasible based upon sliding mode techniques. The methodology can be described by a step-by-step design procedure.

(2) The combination of sliding surface boundary layers, asymptotic observers and reference model "hedging" minimizes the adverse effects of neglected parasitic dynamics upon the control scheme.

(3) In an example focusing upon the longitudinal control of a model of a highly unstable aircraft, the sliding mode design exhibited superior stability and performance robustness as compared to a classical, loop-shaped design. This robustness is attributable to the significantly higher equivalent crossover frequency that can be obtained with the sliding mode approach.

(4) Using reduced-order models of actuator dynamics is a feasible alternative to neglecting them entirely in the design procedure, albeit at the price of higher measurement noise amplification.

(5) Under the assumption of a square, feedback linearizable control architecture, MIMO control formulations are possible with little added complexity compared to SISO formulations.

ACKNOWLEDGEMENT

This research was supported by grants from NASA Langley Research Center, Hampton, VA, USA. The grant technical managers were Barton Bacon and John Davidson.

REFERENCES

1 **Eslinger, R. A.** and **Chandler, P. R**, Self repairing flight control system program overview, *Proceedings of the National Aerospace and Electronics Conference,* IEEE, 1988, pp. 504-511.

2 **Burken, J. J.** and **Burcham, F. W.**, Flight-test results of propulsion-only emergency control system on MD-11 airplane, *Journal of Guidance, Control, and Dynamics*, 1997, **20**, pp. 980-987.

3 **Burcham, F. W., Maine, T.,** and **Wolf, T.,** Flight testing and simulation of an F-15 airplane using throttles for flight control, 1992, AIAA Paper No. 92-4109.

4 **Maybeck, P. S.,** and **Stevens, R. D.,** Reconfigurable flight control via multiple model adaptive control methods, *IEEE Transactions on Aerospace and Electronic Systems,* 1991, **27**, pp. 470-480.

5 **Bodson, M.,** and **Groszkiewicz, J.** Multivariable adaptive algorithms for reconfigurable flight control, *IEEE Transactions on Control Systems Technology,* 1997, **5**, pp. 217-229.

6 **Itkis, U.,** *Control Systems of Variable Structure,* 1976, (Wiley, New York).

7 **Utkin, V. I.,** Variable structure systems with sliding mode, *IEEE Transactions on Automatic Control,* 1977, **(AC-22),** pp. 212-222.

8 **Edwards, C.** and **Spurgeon, S. K.,** *Sliding Mode Control*, 1998, (Taylor & Francis, London).

9 **Hung, J. Y., Weibing, G.** and **Hung, J. C.,** Variable structure control: a survey, *IEEE Transactions on Industrial Electronics,* 1993, **(40)**, pp. 2-23.

10 **Fernandez, B. R.** and **Hedrick, J. K.,** Control of multivariable non-linear systems by the sliding mode method, *International Journal of Control,* 1987, **(46)**, pp. 1019-1040.

11 **Slotine, J.-J. E** and **Li, W.**, *Applied Nonlinear Control,* 1991, (Prentice Hall, Englewood Cliffs, New Jersey).

12 **Lane, S. H.** and **Stengel, R. F.** Flight control design using non-linear inverse dynamics, *Automatica,* 1988, **(24)**, pp. 471-483.

13 **Young, K. D., Utkin, V. I.** and **Ozguner, U.,** A control engineer's guide to sliding mode control, 1999, *IEEE Transactions on Control Systems Technology*, (7), pp. 328-342.

14 **Wells, S. R.** and **Hess, R. A.,** MIMO Sliding mode control for a tailless aircraft – an alternative to reconfigurable architectures, 2002, AIAA paper 2002-4650.

15 **Gilbert, M. G.,** Dynamic modeling and active control of aeroelastic aircraft, 1982, MS thesis, School of Aeronautics and Astronautics, Purdue University.

16 **Hess, R. A.**, Unified theory for aircraft handling qualities and adverse aircraft-pilot coupling, 1997, *Journal of Guidance, Control, and Dynamics,* (**20**), pp. 1141-1148.

17 **Mitchell, D. G., Hoh, R. H., Aponso, B. L. and Klyde, D. H.,** Proposed incorporation of mission-oriented flyign qualities into MIl-STD-1797A, Oct. 1994, WL-TR-94-3162, Wright Laboratory, Wright-Patterson, AFB, OH.

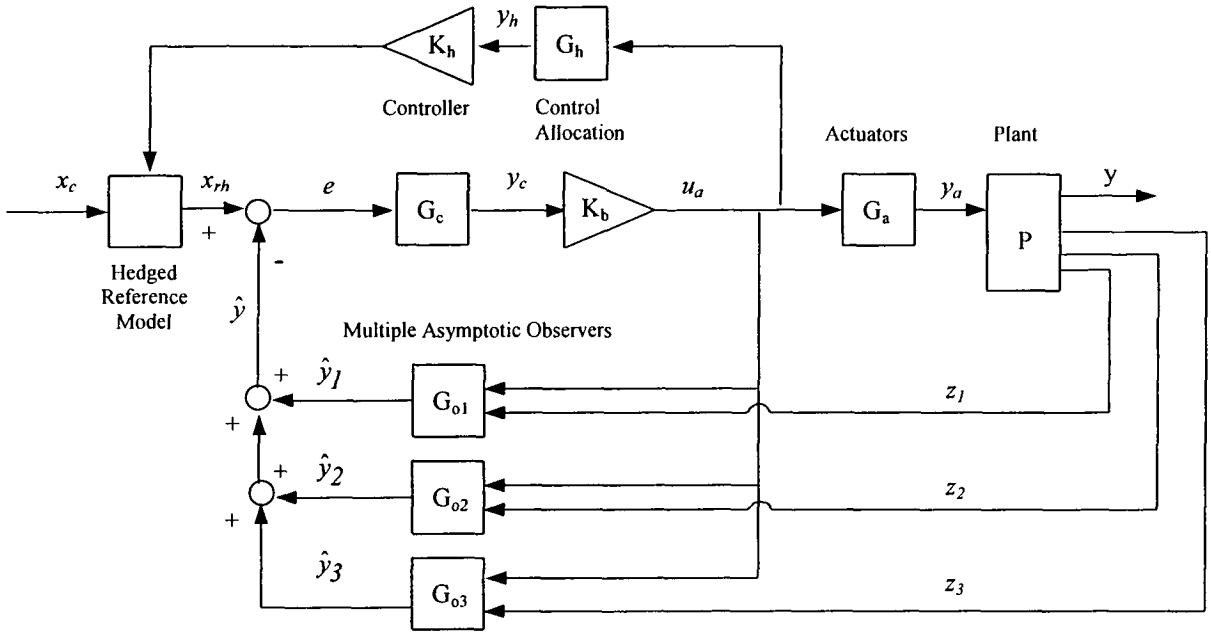

Figure 1 SMC system with observers and reference model hedging

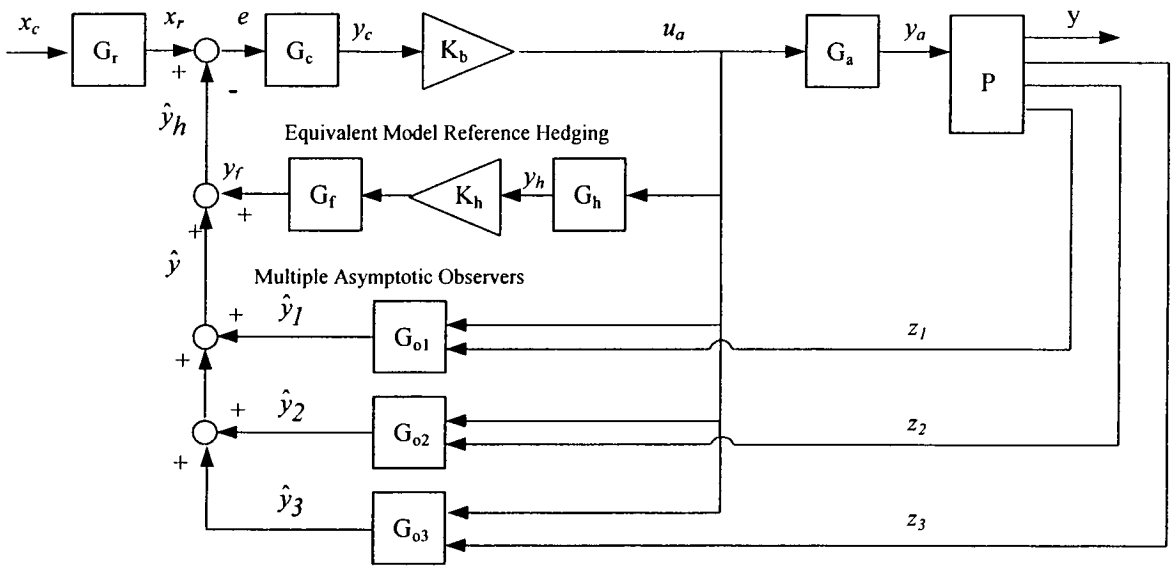

Figure 2 System of Fig. 1 with equivalent model reference hedging

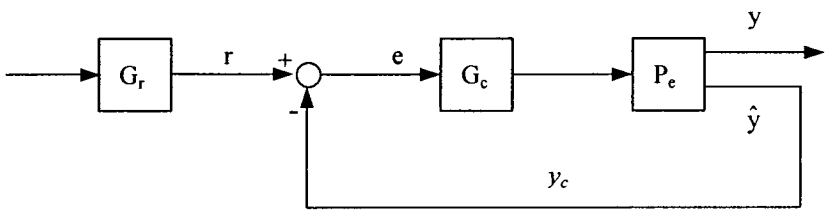

Figure 3 System of Fig. 2 with equivalent plant

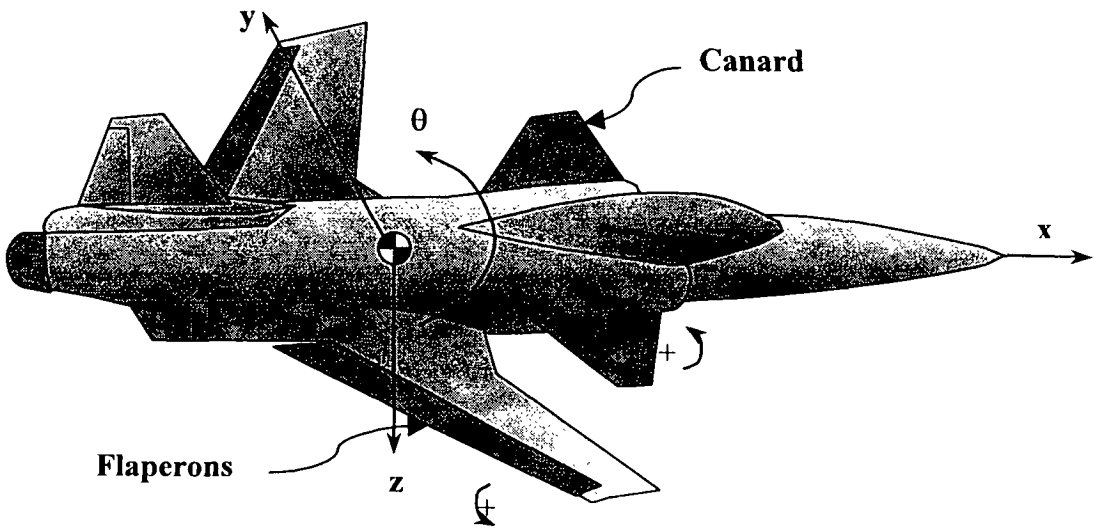

Figure 4 Forward-swept wing vehicle

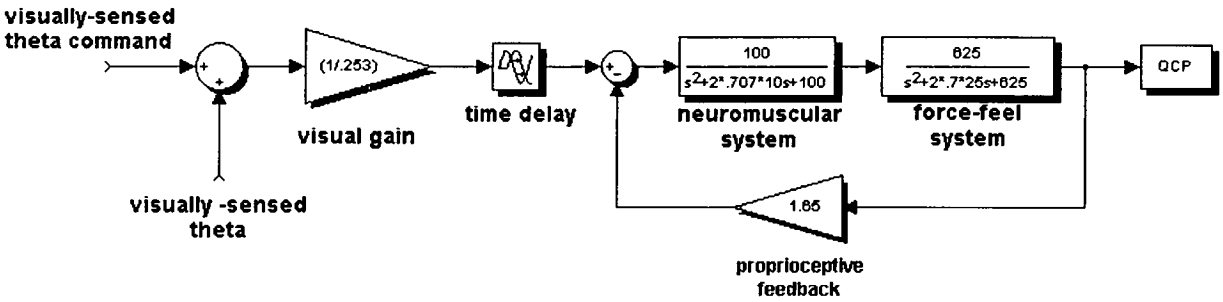

Figure 5 Structural pilot model for pitch-attitude tracking implemented in Simulink®

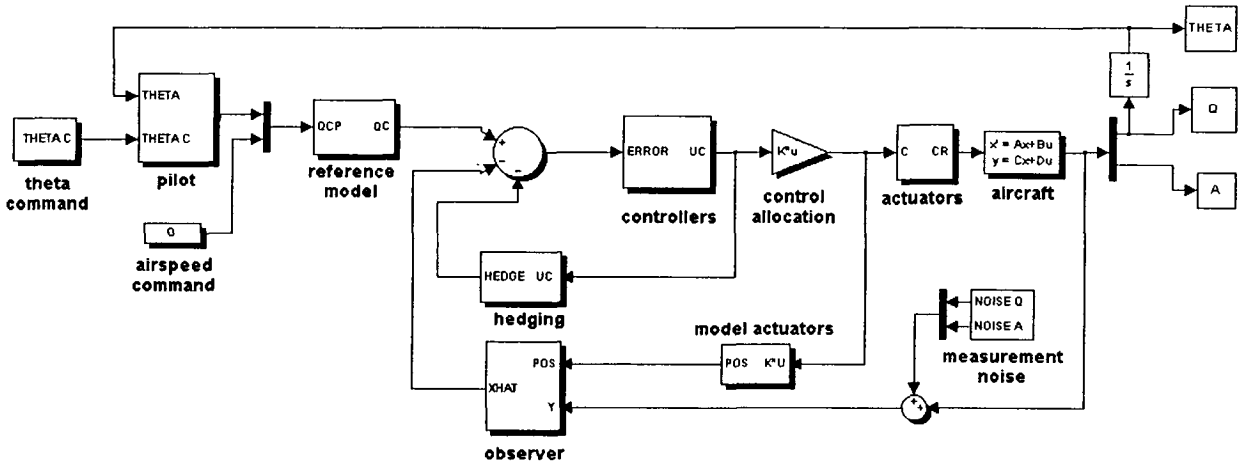

Figure 6 The pilot/vehicle system implemented in Simulink®

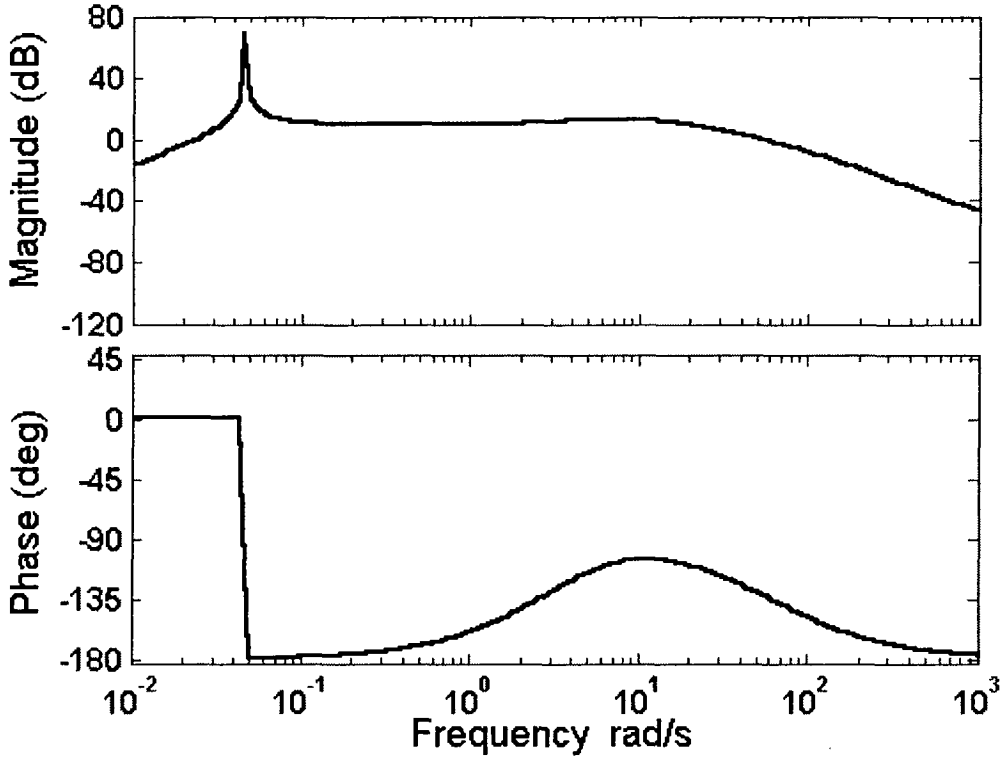

Figure 7 The q/u_{cq} transfer function, first-order actuator dynamics, no aeroelastic modes

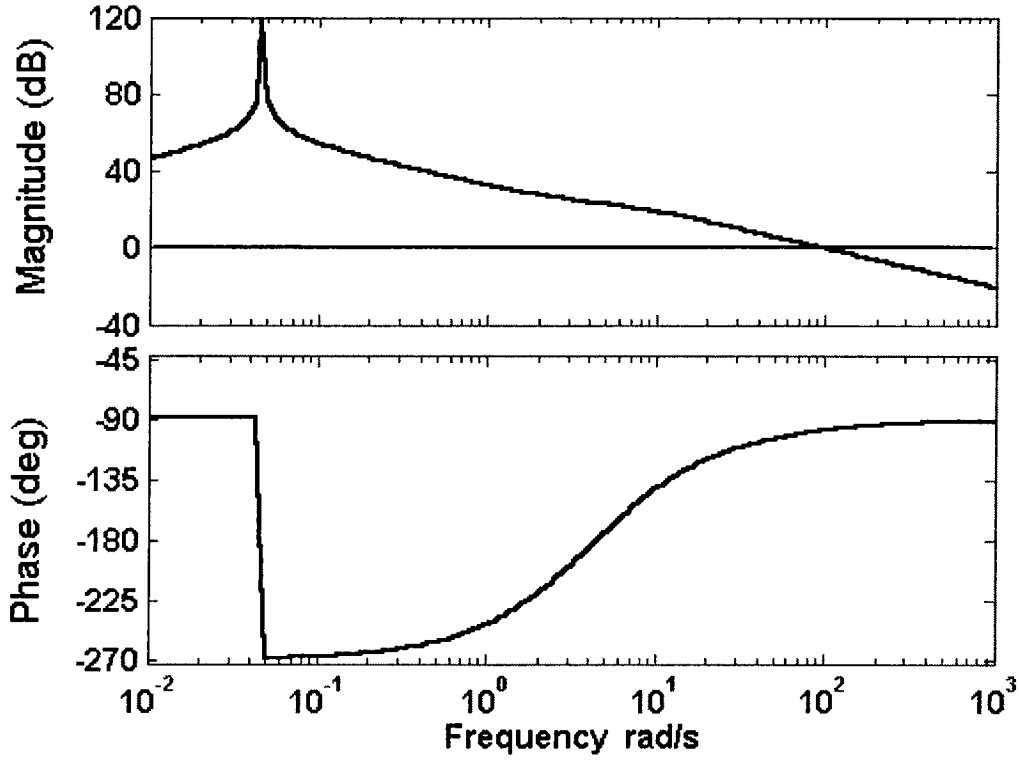

Figure 8 Compensated q – loop system

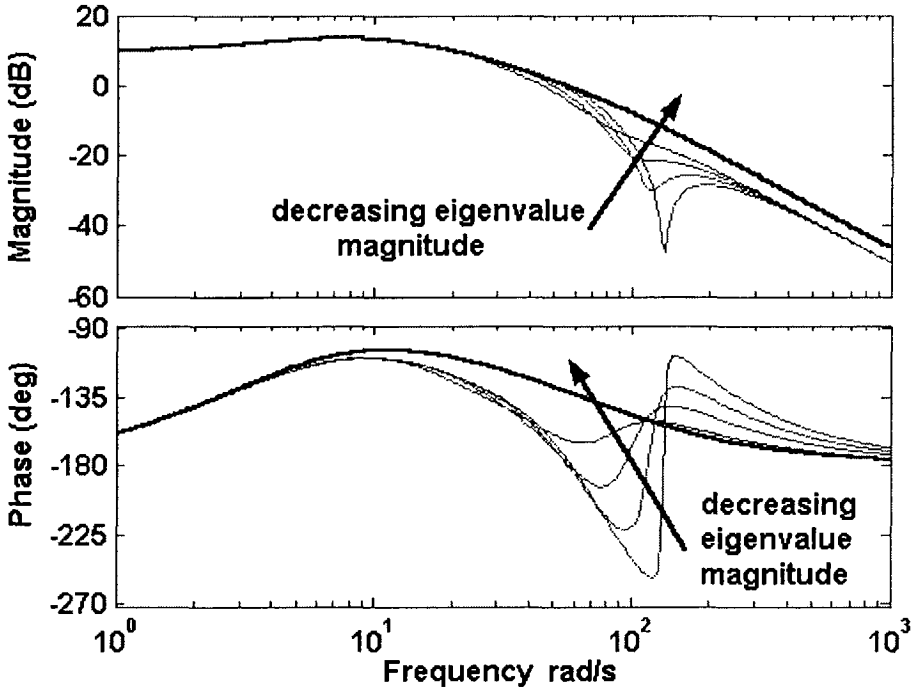

Figure 9 Effect of q-loop observer eigenvalues on $\hat{q}/u_{cq}$

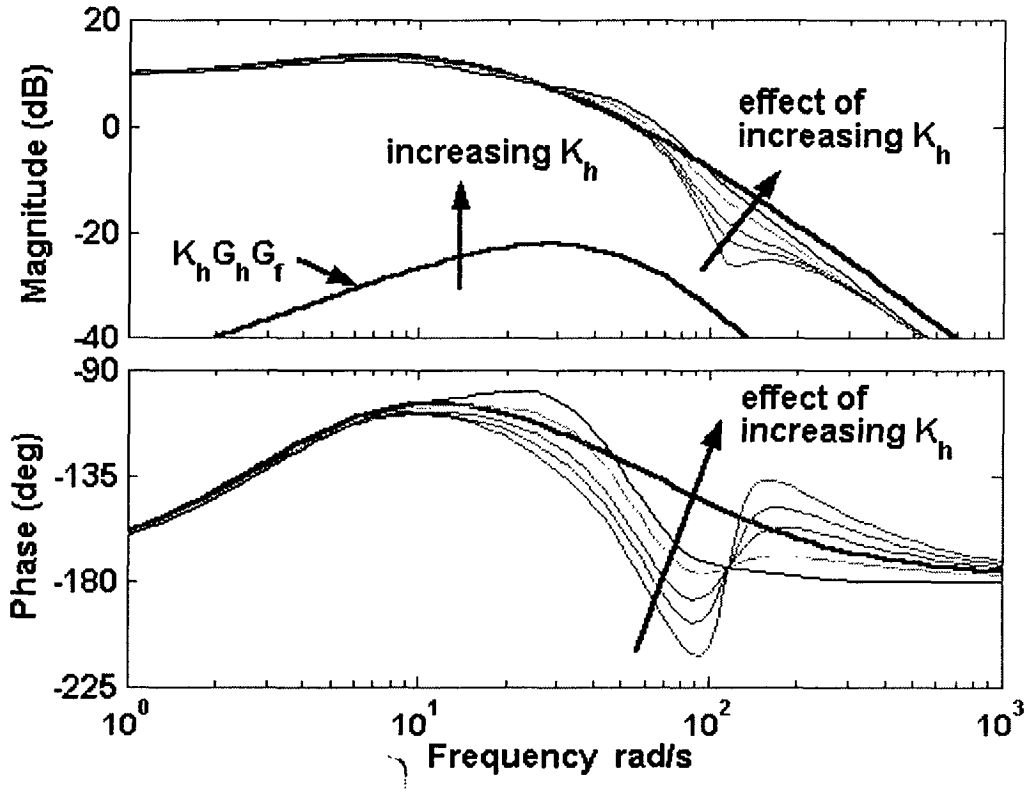

Figure 10 Effect of increasing K_h in refernce model hedging on $\hat{q}/u_{cq}$

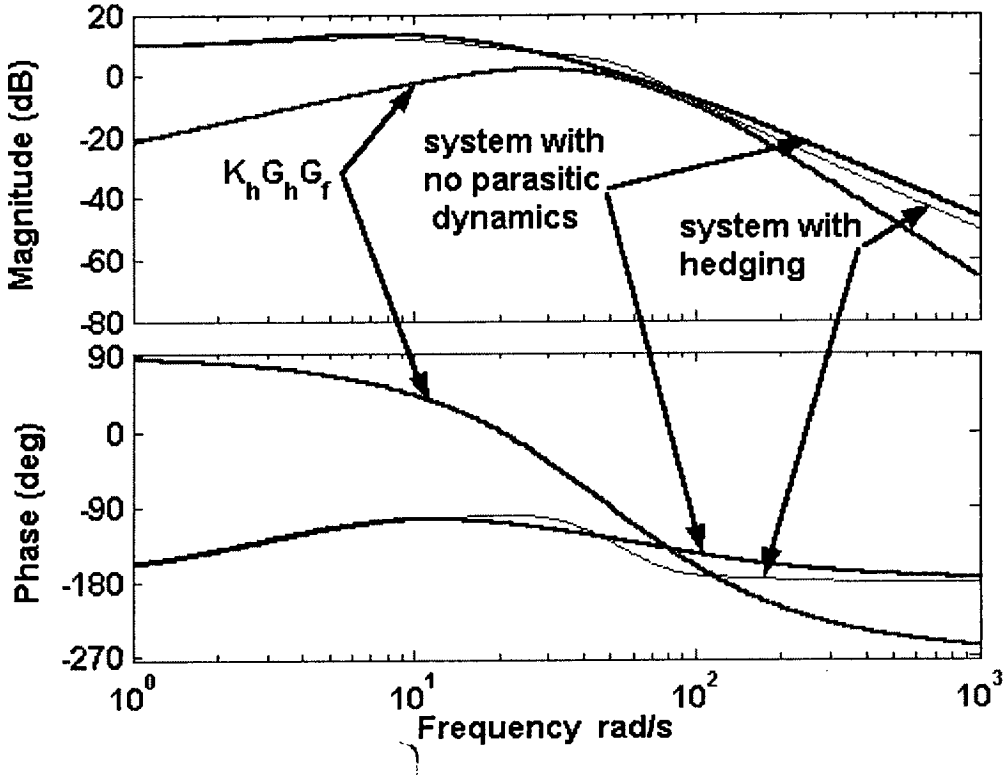

Figure 11 Effect of reference model hedging on $\hat{q}/u_{cq}$, $K_h = 5.2 \cdot 10^5$

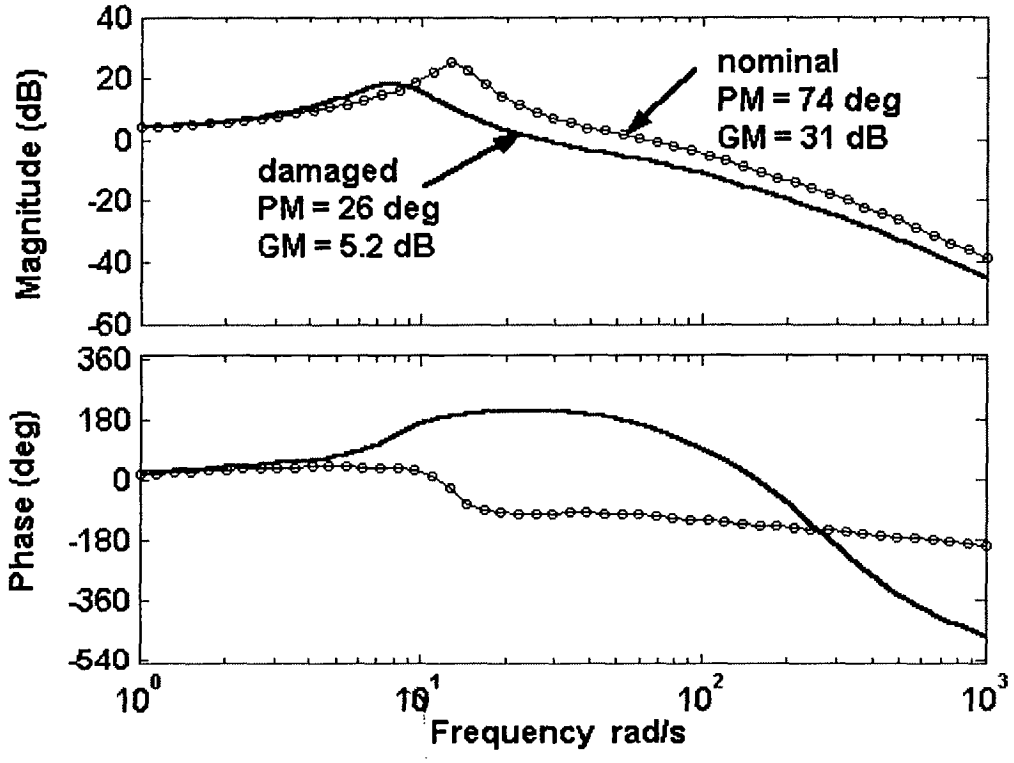

Figure 12 Loop transmissions when loops are cut immediately before canard actuator, nominal and damage condition 1

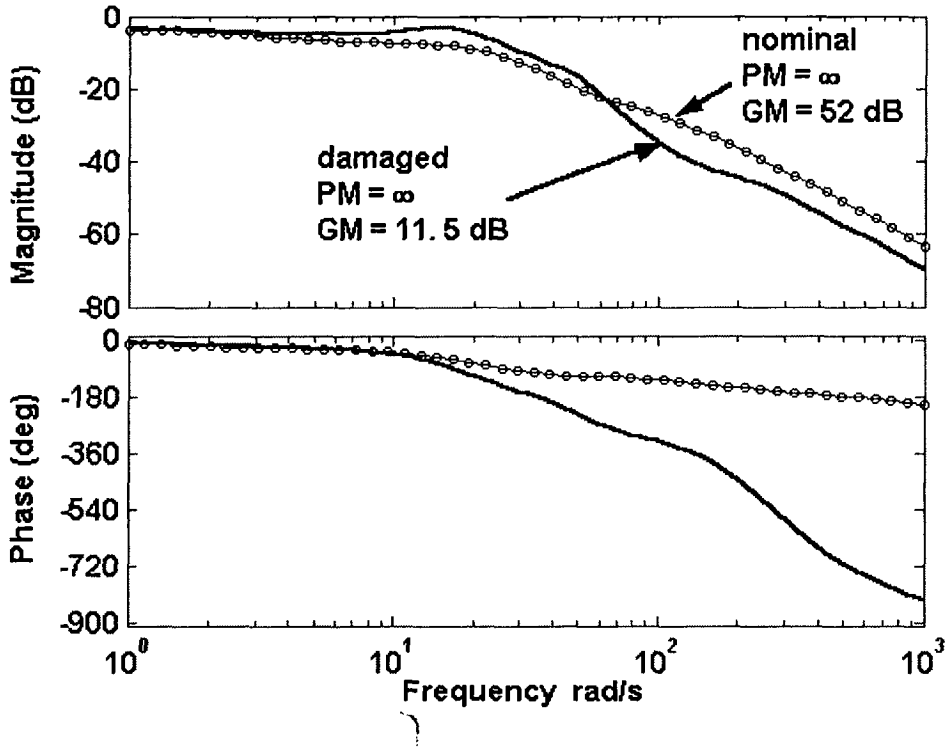

Figure 13 Loop transmissions when loops are cut immediately before flaperon actuator, nominal and damage condition 1

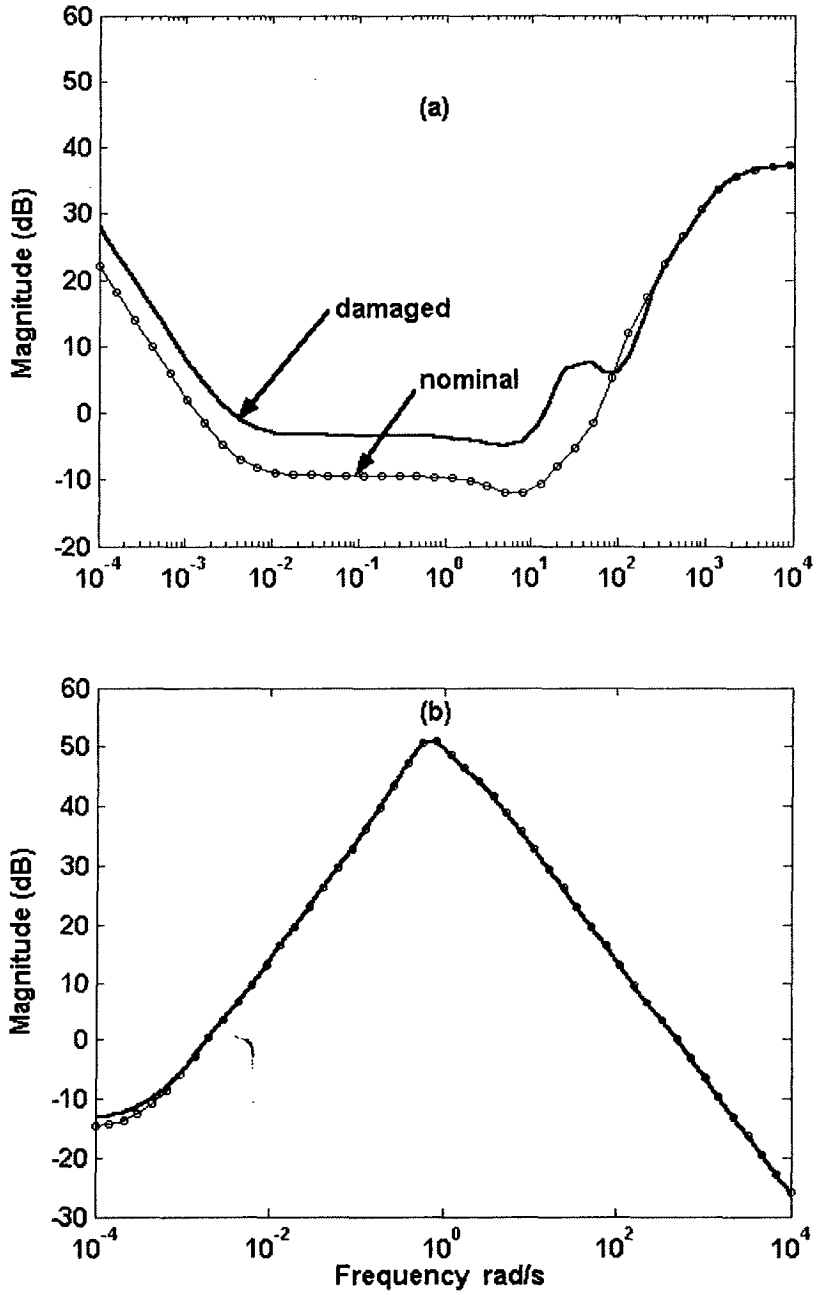

Figure 14 Noise amplification: (a) q_{noise} to u_{cq}; (b) a_{noise} to u_{ca}

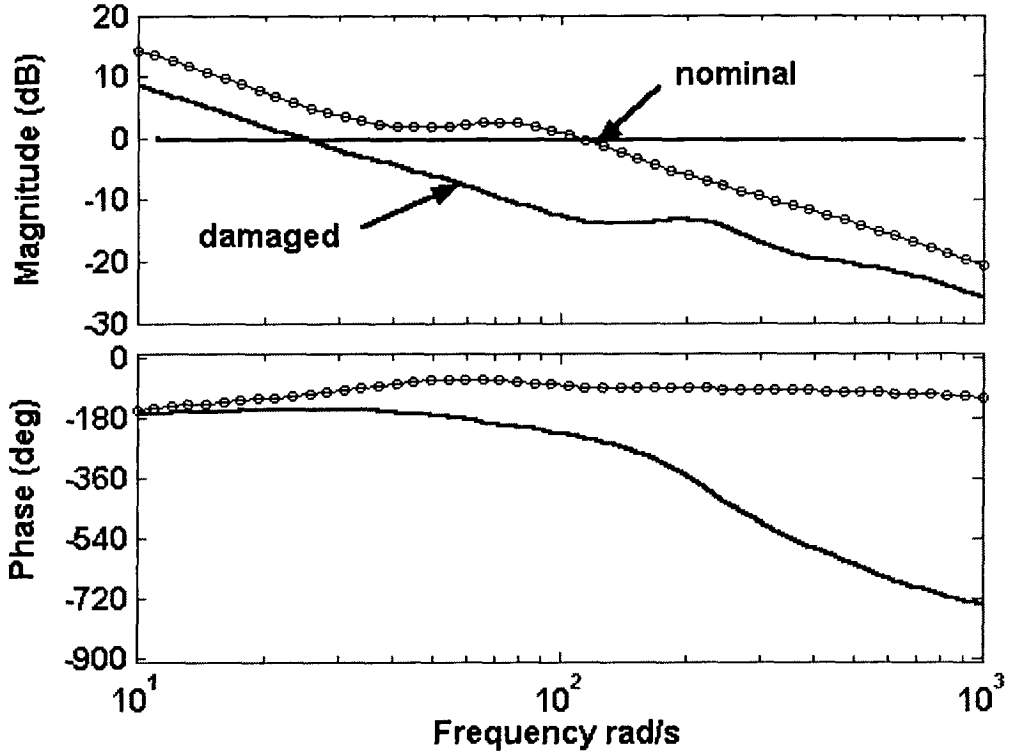

Figure 15 Comparison of L_{equiv} for q-loop, nominal and damaged vehicle, damage condition 1

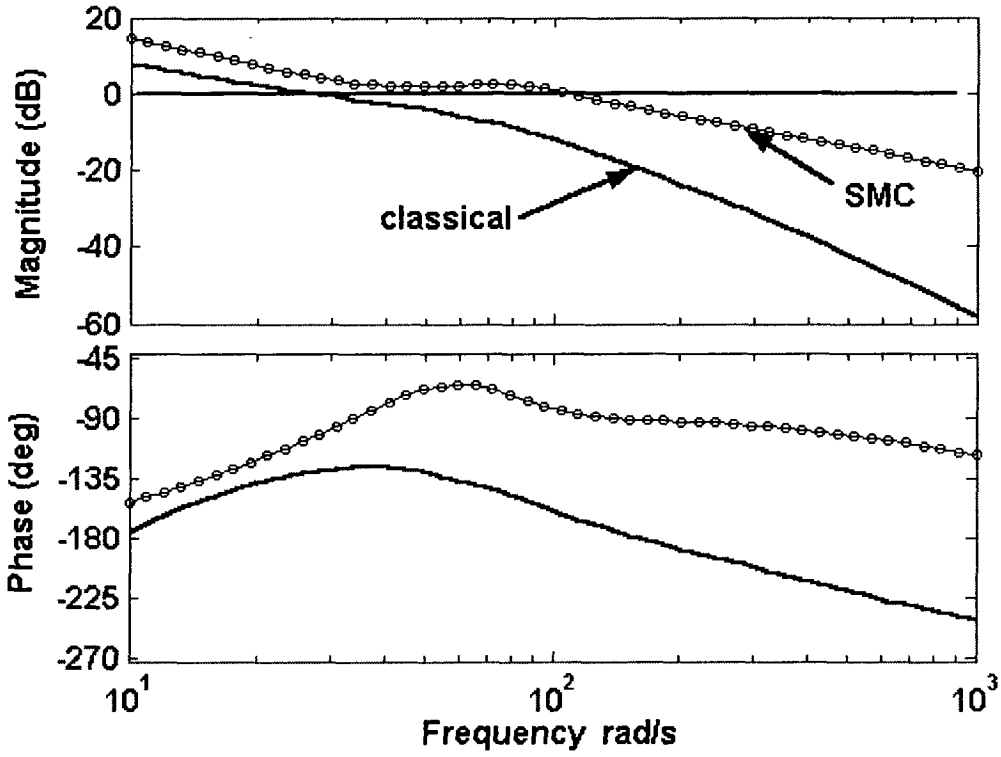

Figure 16 Comparison of L_{equiv} for q-loop, SMC and classical design, nominal systems

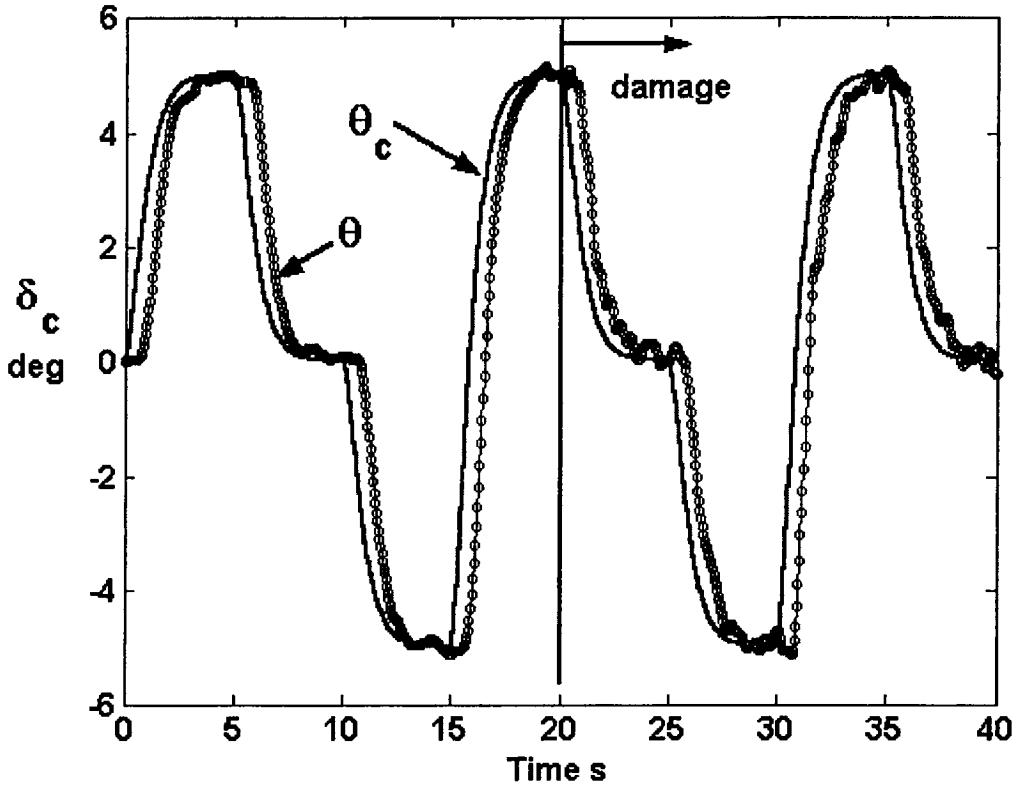

Figure 17 Pitch-attitude pilot/vehicle tracking performance for SMC design, damage condition 1

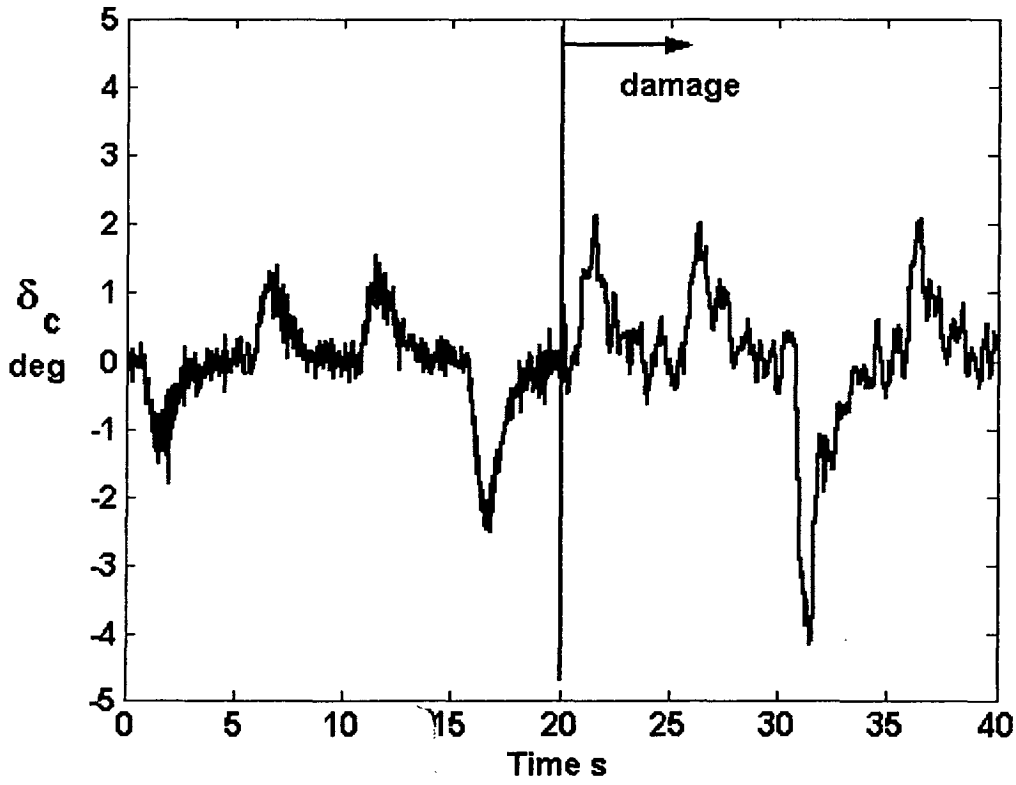

Figure 18 Canard time history for SMC design, damage condition 1

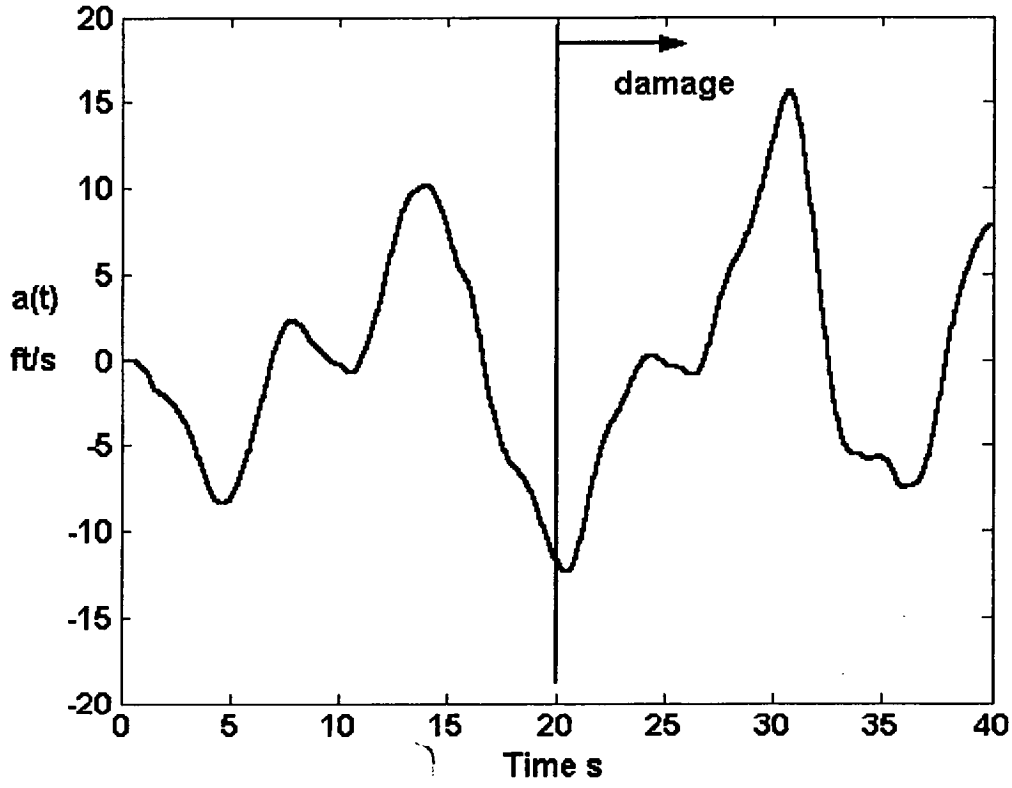

Figure 19 Airspeed deviation time history for SMC design, damage condition 1

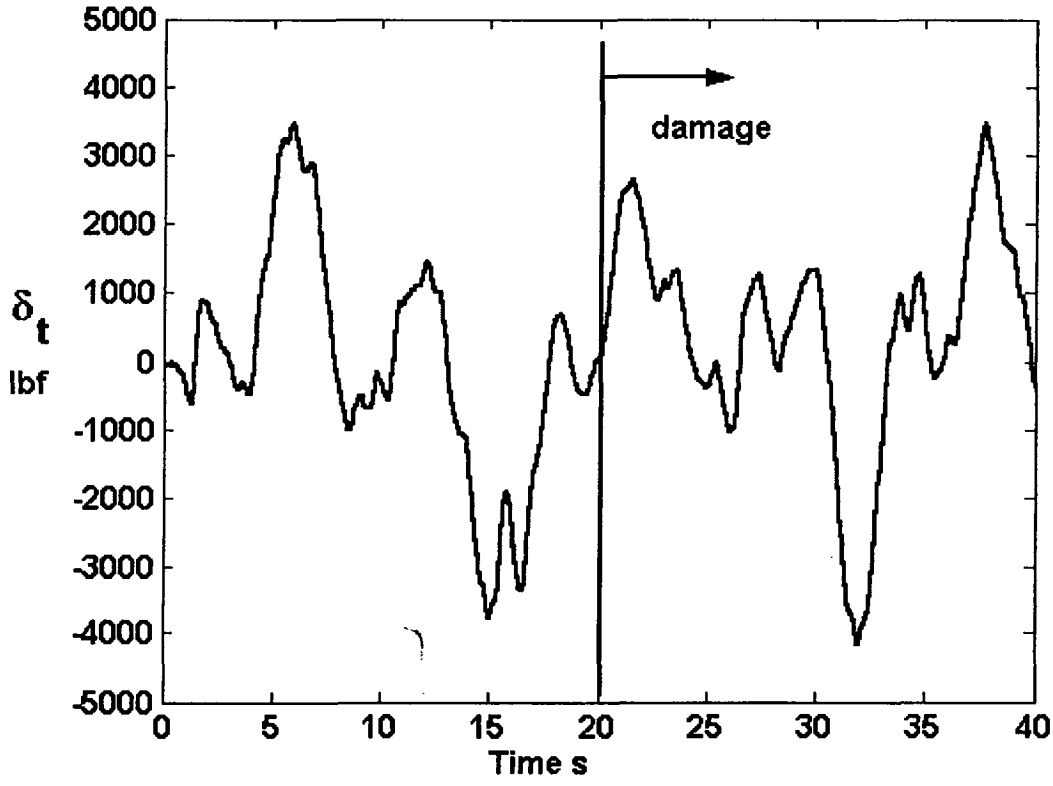

Figure 20 Thrust time history for SMC design, damage condition 1

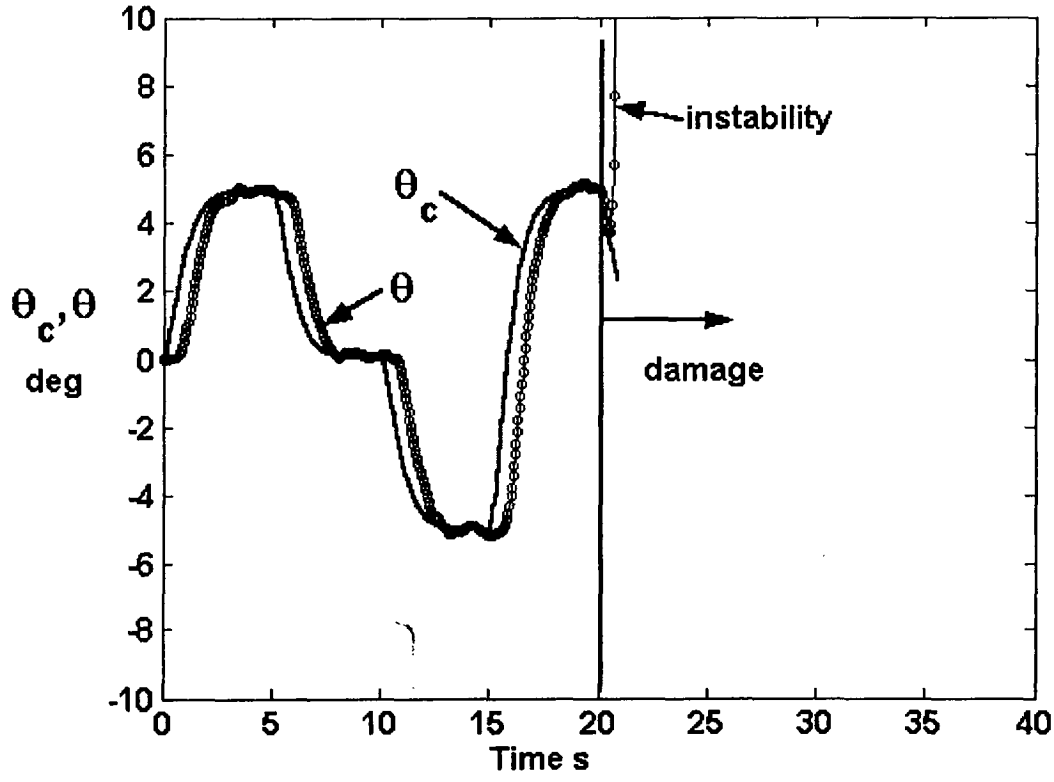

Figure 21 Pitch-attitude pilot/vehicle tracking performance for classical design, damage condition 1

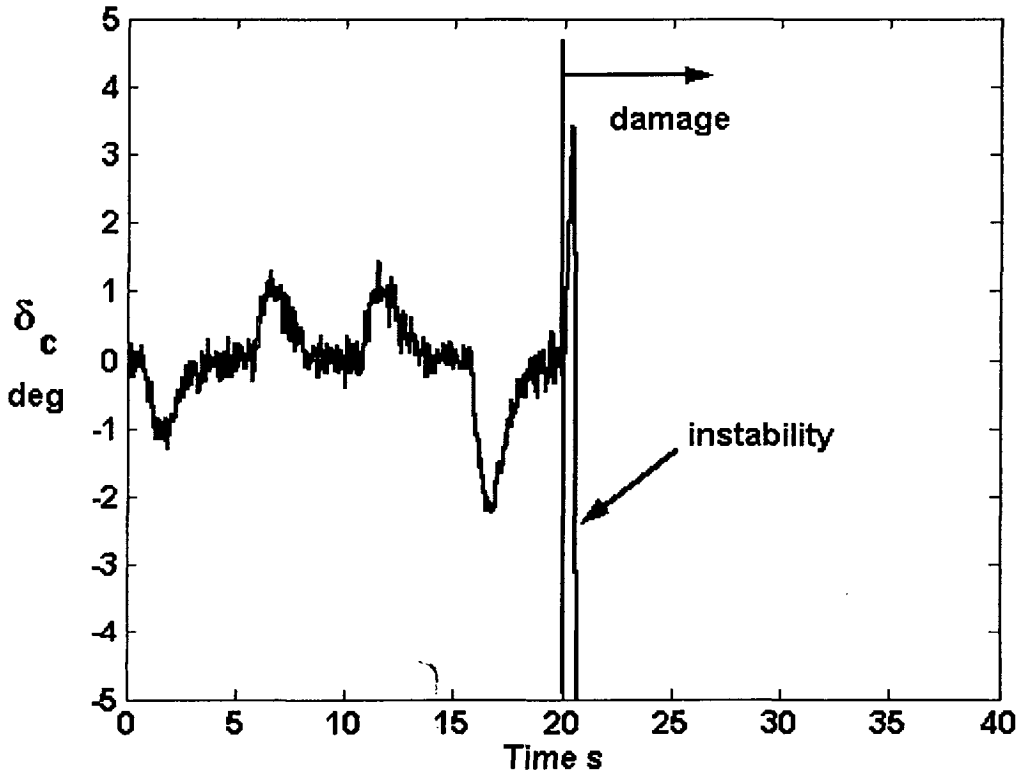

Figure 22 Canard time history for classical design, damage condition 1

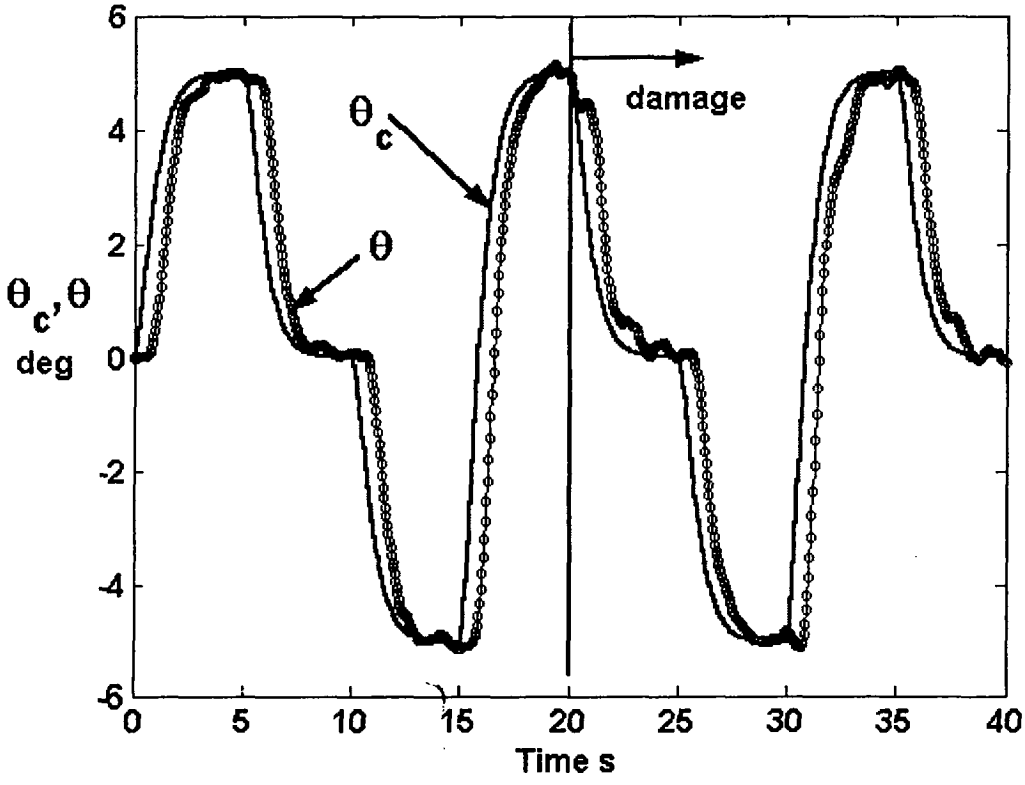

Figure 23 Pitch-attitude pilot/vehicle tracking performance for SMC design, damage condition 2

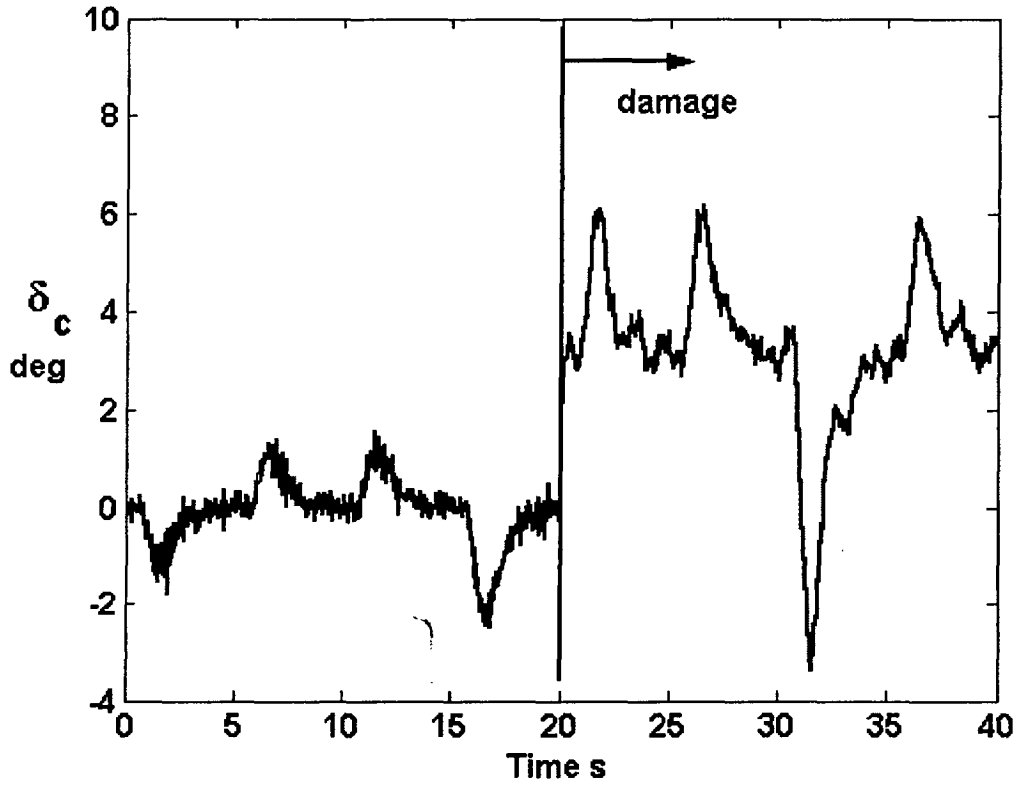

Figure 24 Canard time history for SMC design, damage condition 2

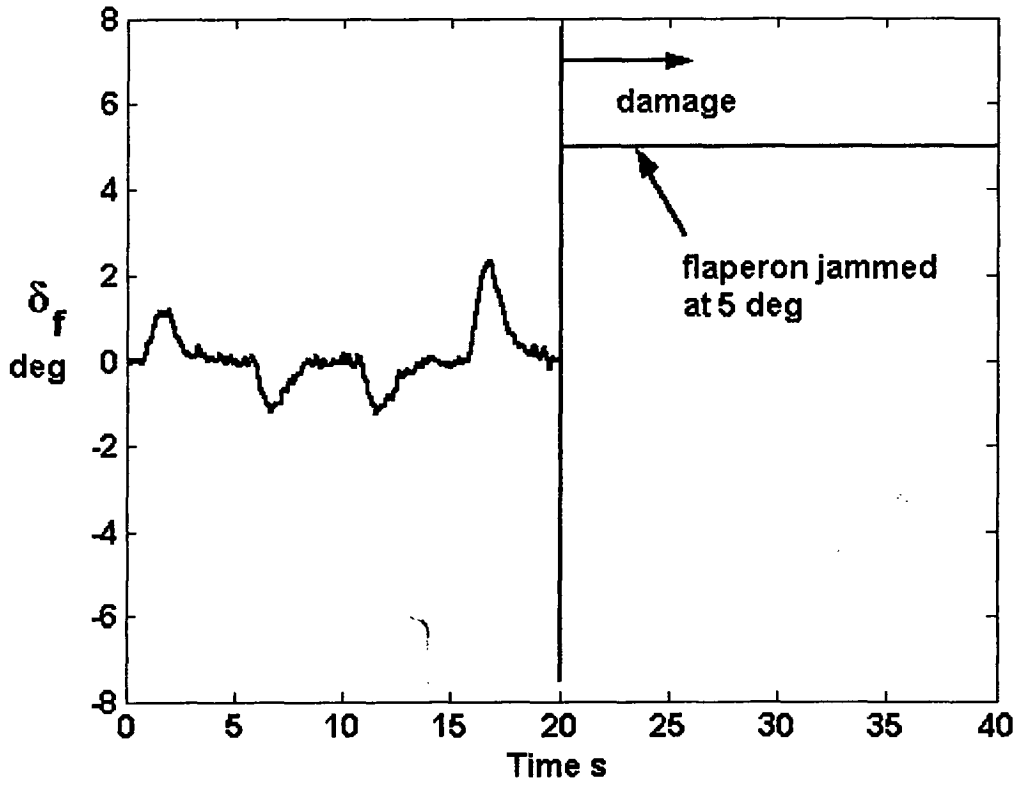

Figure 25 Flaperon time history for SMC design, damage condition 2

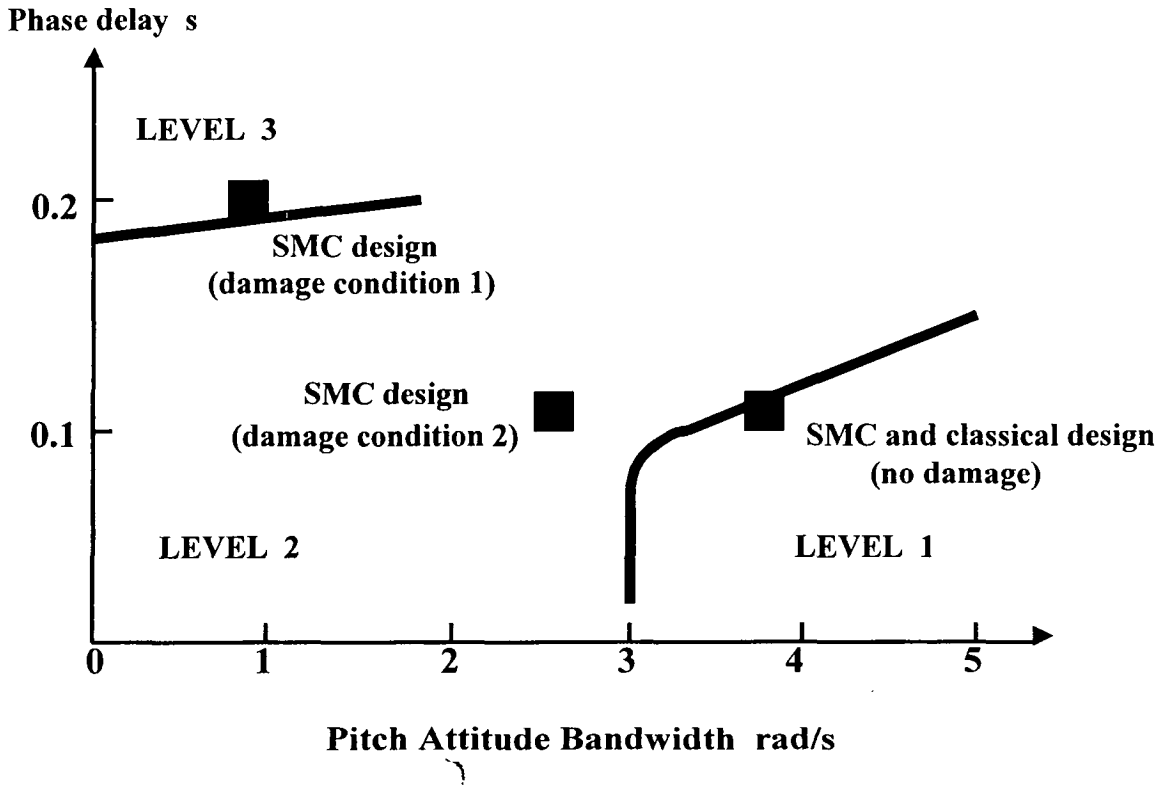

Figure 26 Bandwidth/Phase Delay predictions, aft cg configuration